Manganese Silyl Dihydride Complexes: A Spectroscopic, Crystallographic and Computational Study of Nonclassical Silicate and Hydrosilane Hydride Isomers

Jeffrey S. Price, David J. H. Emslie,* and Bob Berno

Department of Chemistry, McMaster University, 1280 Main St. West, Hamilton, ON, L8S 4M1, Canada

ABSTRACT: Manganese silyl dihydride complexes [$(dmpe)_2MnH_2(SiHR_2)$] {R = Ph (**3a**), R = Et (**3b**)} and [$(dmpe)_2MnH_2(SiH_2R)$] {R = Ph (**4a**), R = ^{n}Bu (**4b**)} were generated by exposure of silylene hydride complexes, [$(dmpe)_2MnH(=SiR_2)$] (**1a**: R = Ph, **1b**: R = Et), and disilyl hydride complexes, [$(dmpe)_2MnH(SiH_2R)_2$] (**2a**: R = Ph, **2b**: R = ^{n}Bu), respectively, to H_2 at room temperature. In solution, **3a-b** and **4a-b** exist as an equilibrium mixture of a *central* isomer with a meridional H–Si–H arrangement of the silyl and hydride ligands {this isomer may be considered to contain an η^3-coordinated silicate ($H_2SiR_3^-$) anion}, and a *transHSi* isomer with *trans*-disposed hydride and nonclassical hydrosilane ligands (the latter is the result of significant but incomplete hydrosilane oxidative addition). Additionally, DFT calculations indicate the thermodynamic accessibility of *lateralH_2* and *transH_2* isomers with *cis*- and *trans*-disposed silyl and dihydrogen ligands, respectively. Compounds **3a** and **4a** crystallized as the *central* isomer, whereas **4b** crystallized as the *transHSi* isomer. Bonding in the *central* and *transHSi* isomers of **3a-b** and **4a-b** was further investigated through ^{29}Si_edited ^{1}H–^{1}H COSY solution NMR experiments to determine both the sign and magnitude of $J_{29Si,1H}$ coupling (negative and positive values of $J_{29Si,1H}$ are indicative of dominant 1-bond and 2-bond coupling, respectively). These experiments afforded $J_{29Si,1H}$ coupling constants of –47 Hz for η^3-(H_2SiR_3) in the *central* isomer of **3b** (calcd. –40 to –47 for **3a-b** and **4a-b**), –38 to –54 Hz for η^2-(R_3Si–*H*) in the *transHSi* isomer of **3a-b** and **4a-b** (calcd. –26 to –47 Hz), and 5 to 9 Hz for the terminal manganese hydride ligand in the *transHSi* isomer of **3b** and **4a-b** (calcd. 12 to 14 Hz for **3a-b** and **4a-b**), experimentally supporting the nonclassical nature of bonding in the *central* and *transHSi* isomers.

INTRODUCTION

Transition metal hydrosilane complexes are a class of sigma complex important in many chemical transformations, especially those involving formation of Si–C bonds.[1-3] Isolated examples of hydrosilane complexes are far less common than related dihydrogen complexes, despite the fact that the first hydrosilane complex was reported by Graham *et al.* in 1969,[4] 15 years before Kubas' report of the first H_2 complex.[5] Upon oxidative addition of the Si–H bond, classical silyl hydride complexes (with two separate 2c-2e bonds, as opposed to a single 3c-2e bond) are formed. However, as early as 1971, Graham reported a monometallic silyl hydride complex with significant interligand Si–H bonding.[6] These nonclassical hydrosilane complexes have been the subject of a number of reviews,[7-9] and from a molecular orbital perspective, they are typically described using a modification of the Dewar-Chatt-Duncanson bonding model, with concomitant σ donation and π backdonation to/from the metal (Figure 1). A variety of terms have been employed to describe these intermediate complexes,[10,11] and comprehensive studies by a number of groups, including those of Nikonov,[12-19] Sabo-Etienne,[9,20-25] and Scherer,[26-28] have shown that a continuum exists between σ-hydrosilane complexes involving minimal π-backdonation, and classical silyl hydride complexes. This continuum follows the oxidative addition/reductive elimination reaction coordinate, with progressively weakening Si–H interactions indicative of a greater degree of oxidative addition. In this work we use the term "nonclassical" to refer to complexes in the central region of this continuum, where the extent of oxidative addition is significant but incomplete. Such nonclassical complexes provide snapshots along the oxidative addition pathway, which is one of the most important classes of organometallic reaction.

Analyses of nonclassical hydrosilane complexes have naturally focused on the strength of the Si–H interaction, from which the degree of oxidative addition can be inferred. These strengths have often been determined computationally,[13,16,17,21,26,28-30] while experimental studies have primarily involved solid-state structural determination of the Si–H distance. However, care must be taken when discussing Si–H distances determined by X-ray crystallography, due to difficulties associated with accurately locating hydrogen atoms from the difference map. More importantly, it has been observed that significant changes in the degree of oxidative addition (based on $J_{Si,H}$ coupling constants; *vide infra*) may only yield very small changes in the Si–H distance, and Si–H distances below the sum of the van der Waals radii may be steric in origin, so do not necessarily imply Si–H bonding.[8] Furthermore, there is no intuitive boundary to define nonclassical hydrosilane complexes with respect to either σ-hydrosilane or classical silyl hydride complexes, and different Si–H distance ranges have been suggested to correspond to these intermediate complexes. The lower end of this range is often considered to be 1.8 Å, while distances of 2.1 and 2.4 Å have been proposed by Nikonov[8] and Sabo-Etienne[9] respectively to correspond to the upper limit.

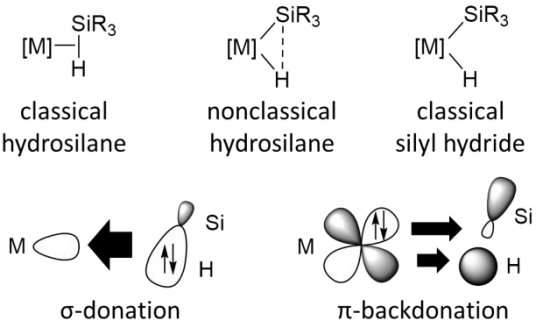

Figure 1. Top: From left to right, structures of σ-hydrosilane, nonclassical hydrosilane, and classical silyl hydride complexes. Bottom: Classical Dewar-Chatt-Duncanson model of σ donation and π backdonation from/to a hydrosilane ligand.

Spectroscopically, ^{1}H and ^{29}Si NMR chemical shifts are not especially useful to evaluate the extent of hydrosilane oxidative addition, given that similar ranges of values are observed for σ-hydrosilane, classical silyl hydride, and nonclassical hydrosilane complexes.[9] By contrast, ^{29}Si–^{1}H NMR coupling constants ($J_{Si,H}$) can be used as a sensitive tool to measure the nature of interligand Si–H interactions.[31] However, it is important to recognize that 1-bond Si–H coupling has a negative sign, whereas 2-bond Si–H coupling has a positive sign, so $J_{Si,H}$ passes through zero on the continuum from a σ-hydrosilane to a classical silyl hydride complex, and proper placement of a complex along this continuum requires knowledge both of the magnitude and sign of $J_{Si,H}$.[27,28,30,32]

The magnitude of $J_{Si,H}$ can typically be obtained via 1D ^{1}H or ^{29}Si NMR spectroscopy, but measurement of the sign is more difficult. One method used in the literature is spin tickling,[30] but individual multiplet signals must be well-resolved, and its analysis is not conceptually straightforward.[33] Recently, Scherer reported an alternative spectroscopic method for determining the sign (and magnitude) of $J_{Si,H}$ in silyl hydride/hydrosilane complexes where the silicon center also features a terminal Si–H bond. This method relies upon 2D ^{1}H–^{1}H COSY data, using the negative coupling constants of the terminal Si–H bond[34] as an internal reference to definitely determine the sign of $J_{Si,H}$ from the orientation of ^{29}Si satellites associated with a cross-peak of interest (*vide infra*).[27,28] While there is still some debate, $J_{Si,H}$ values ranging from 0 to –70 Hz are commonly considered to indicate activated Si–H bonds in nonclassical silyl hydride complexes, where $^{1}J_{Si,H}$ coupling (transmitted via the molecular orbital involved in σ-donation), dominates over $^{2}J_{Si,H}$ coupling (associated with π-backdonation). Values more negative than –70 Hz are indicative of σ-hydrosilane complexes with limited π-backdonation, and positive values are indicative of silyl hydride complexes with very weak or non-existent Si–H interactions).[1,28,30]

A range of transition metal complexes have also been isolated containing a silyl group accompanied by more than one hydride ligand. The generic term 'silyl dihydride' is frequently used to describe complexes with one SiR_3 and two hydride moieties interacting with a metal center, regardless of the extent of any interligand Si–H interaction(s). Within this class of complexes, a variety of examples have been observed where a single silyl ligand simultaneously interacts with multiple hydride ligands.[16,35,36] In 1989, Crabtree *et al.* first proposed such a complex as a potential intermediate in the dynamic exchange between the terminal metal hydride and bridging hydrosilyl environments in $[(Ph_3P)_2IrH_2(\eta^2\text{-}HSiEt_3)]^+$.[37] Then, in 1990, the same group reported the first examples of transition metal (Re) complexes featuring multiple (four or two) hydride ligands interacting with a single silyl ligand (Figure 2, a and b), though the hydride atoms were not crystallographically located.[38] Five years later, Klabunde and Radonovich *et al.* reported X-ray crystal structures for a pair of chromium disilyl dihydride complexes with short distances between one of the silyl ligands and two neighboring hydride ligands (1.75(7) and 1.60(6) Å for one, 1.66(4) and 1.87(4) Å for the other; c in Figure 2), though the authors stopped short of stating that two Si–H interactions were present due to significant errors in the bond distances and potential involvement of the second silyl ligand in the bonding scheme.[39] Then, in 1999, Sabo-Etienne *et al.* reported a Ru complex featuring a silyl ligand with two adjacent hydride co-ligands (d in Figure 2), with short Si–H distances of 1.72(3) and 1.83(3) Å determined by X-ray diffraction.[40] Over the past two decades, approximately a dozen crystallographically characterized monometallic transition metal silyl dihydride complexes have been reported to feature interactions between a silyl ligand and two hydride ligands, and are often referred to as silicate ($H_2SiR_3^-$) complexes.[15,18,19,22,39-45] These complexes highlight the potential for silicon hypervalency in transition metal complexes, and are of interest as models in the heterolytic splitting of hydrosilanes on metal centers.[7]

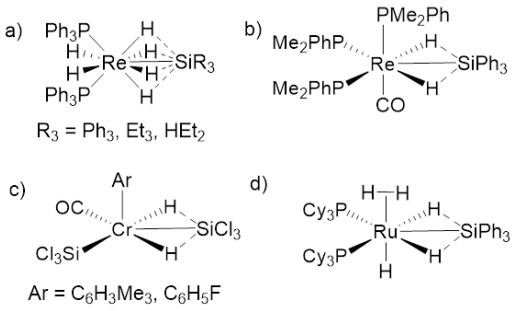

Figure 2. Early examples of complexes reported to involve multiple Si–H interactions to the same silicon center.[38-40]

Herein we discuss the synthesis and characterization of the silyl dihydride complexes $[(dmpe)_2MnH_2(SiHR_2)]$ {R = Ph (**3a**), R = Et (**3b**)} and $[(dmpe)_2MnH_2(SiH_2R)]$ {R = Ph (**4a**), R = ^{n}Bu (**4b**)}, with an examination of the nature of Si–H interactions in different geometric isomers via NMR spectroscopy (including determination of the sign and magnitude of $J_{Si,H}$) combined with X-ray diffraction and DFT calculations.

RESULTS AND DISCUSSION

Previously, our group communicated the synthesis of the silyl dihydride complexes $[(dmpe)_2MnH_2(SiHR_2)]$ (**3a**: R = Ph, **3b**: R = Et) via reactions of the silylene hydride complexes $[(dmpe)_2MnH(=SiR_2)]$ (**1a**: R = Ph, **1b**: R = Et) with H_2 (Scheme 1).[46] In this work, reactions of $[(dmpe)_2MnH(SiH_2R)_2]$ (**2a**: R = Ph, **2b**: R = ^{n}Bu)[47] with H_2 yielded $[(dmpe)_2MnH_2(SiH_2R)]$ (**4a**: R = Ph, **4b**: R = ^{n}Bu) (Scheme 1), affording a family of silyl dihydride complexes (**3a-b** and **4-b**) differing in the number and nature of the hydrocarbyl substituents on silicon. Both of these reactions presumably proceed via a low-coordinate silyl intermediate "$(dmpe)_2Mn(SiH_{3-x}R_x)$", generated either by 1,1-insertion from silylene hydride complexes **1a-b**, or hydrosilane reductive elimination from disilyl hydride complexes **2a-b**. Thermal decomposition of **2a-b** (12h

at 90 °C) also yielded **4a-b** as the dominant manganese complexes in solution, accompanied by R_2SiH_2 (R = Ph or ^{n}Bu) and other unidentified products, although the mechanism for this reaction is unknown.

Scheme 1. Syntheses of [(dmpe)$_2$MnH$_2$(SiHR$_2$)] {R = Ph (**3a**), R = Et (**3b**)} and [(dmpe)$_2$MnH$_2$(SiH$_2$R)] {R = Ph (**4a**), R = ^{n}Bu (**4b**)}.

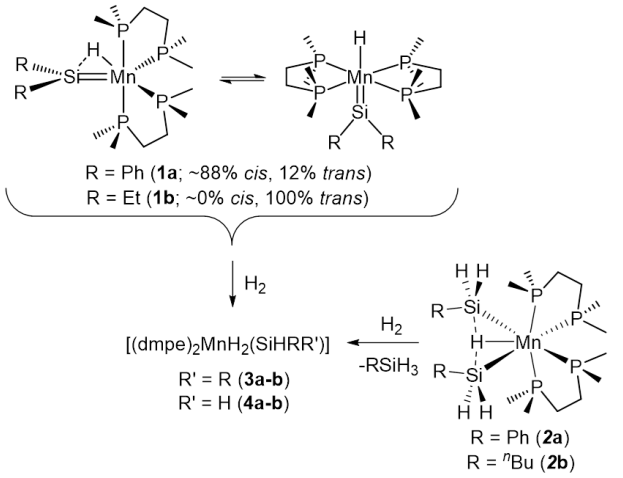

1D NMR Characterization: Room temperature solution NMR spectra (^{1}H, ^{13}C, and ^{31}P)[48] of **3a-b**[46] and **4a-b** display very broad signals indicative of multiple isomers in rapid equilibrium. However, upon cooling, NMR spectra corresponding to both a low symmetry (apparent C_2 symmetry) and a high symmetry (apparent C_{2v} symmetry) isomer were observed (shown for **4a-b** in Figure 3).

NMR spectra for the low symmetry isomer of **3a-b**[46] and **4a-b** feature one low frequency Mn*H* ^{1}H NMR resonance at –12.5 to –12.8 ppm, integrating to two protons, one (**3a-b**) or two (**4a-b**) terminal Si*H* resonance(s) (6.0-6.6 ppm for **3a** and **4a**; 5.0-5.4 ppm for **3b** and **4b**), two ^{31}P NMR resonances (71.0-75.2 ppm), and a single ^{29}Si resonance (10.0 ppm for **3a**, 14.2 ppm for **3b**, –15.7 ppm for **4a**, and –22.0 ppm for **4b**). The two relatively broad ^{31}P NMR signals, and the complex ^{31}P coupling pattern of the Mn*H* signals, are indicative of a disphenoidal arrangement of the phosphorus donors. These data are consistent with a *central* isomer (Scheme 2) featuring a meridional H–Si–H bonding motif involving the silyl and metal hydride ligands (as opposed to a *lateral* isomer with an H–H–Si bonding motif; *vide infra*).

In contrast, low temperature NMR spectra for the high symmetry isomer of **3a-b**[46] and **4a-b** consist of *two* low frequency Mn*H* ^{1}H NMR resonances located between –10.9 to –14.4 ppm (1H each), a single terminal Si*H* ^{1}H NMR resonance {4.7-6.2 ppm; integrating to 1H (**3a-b**) or 2H (**4a-b**)}, and single ^{31}P NMR (77.5-78.5 ppm) and ^{29}Si NMR (23.8 ppm for **3b**; –1.6 ppm for **4a**; –6.9 ppm for **4b**; not located for **3a** due to the low concentration of this isomer) resonances. The single sharp ^{31}P NMR signal and pentet coupling pattern of the higher frequency Mn*H* signal in this isomer of **3a-b** and **4a-b** ($^2J_{H,P}$ = 52-56 Hz) are indicative of two equivalent dmpe ligands lying in a plane with a hydride ligand in an apical site.[49] By contrast, the $^2J_{P,H}$ coupling constants for the lower frequency Mn*H* signal in the same isomer of **3b** and **4a-b** are significantly smaller (22-23 Hz; the analogous signal in **3a** was a multiplet from which $^2J_{P,H}$ could not be determined), consistent with literature examples of $^2J_{P,H}$ for the proton involved in η^2-(H–SiR$_3$) coordination in nonclassical hydrosilane complexes.[50] These data are consistent with a *transHSi* isomer (Scheme 2) featuring *trans*-disposed hydride and nonclassical hydrosilane ligands (as opposed to a *transH$_2$* isomer with *trans* disposed silyl and dihydrogen ligands; *vide infra*), with rapid rotation of the hydrosilane ligand about the Mn–(hydrosilane centroid) axis.

Scheme 2. Isomers of [(dmpe)$_2$MnH$_2$(SiHR$_2$)] {R = Ph (**3a**), R = Et (**3b**)} and [(dmpe)$_2$MnH$_2$(SiH$_2$R)] {R = Ph (**4a**), R = ^{n}Bu (**4b**)} observed in solution.

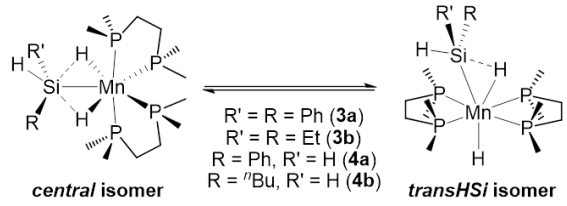

The *central*:*transHSi* ratios observed by NMR spectroscopy are 87:13 for **3a** (271 K), 75:25 for **3b** (229 K), 62:38 for **4a** (186 K), and 27:73 for **4b** (205 K). To our knowledge, this is only the second report of an equilibrium between two silyl dihydride isomers which differ in whether the silyl group interacts with one or both hydride co-ligands; in 2006 Sakaba reported a pair of isostructural tungsten silyl dihydride complexes, [(CO)$_2$Cp*WH$_2$(SiHRPh)] (R = H, Ph), existing in solution as an equilibrium between two isomers; one complex crystallized as an isomer with two close Si–H interactions (1.91(3) and 2.00(4) Å), while the other crystallized as an isomer with a single close Si–H interaction (2.02(4) Å).[51]

Interconversion between the *central* and *transHSi* isomers of **3a-b** and **4a-b** could hypothetically involve initial HSiR$_3$ or H$_2$ dissociation. However, the terminal Si*H* environment(s) and the metal hydride environments do not undergo facile exchange at room temperature; upon selective deuteration of the metal hydride environment in **3b**, **4a**, and **4b**, no deuterium incorporation into the terminal Si*H* environment was observed after 12 hours in solution.[52] This indicates that isomerization (which is rapid at room temperature for both **3a-b** and **4a-b**), does not involve hydrosilane dissociation to form 5-coordinate "(dmpe)$_2$MnH" as an intermediate. Likewise, addition of D$_2$ to **4a** did not result in any observable deuteration of the complex after 72h in solution at room temperature, suggesting that H$_2$ dissociation to form a 5-coordinate "(dmpe)$_2$Mn(SiR$_3$)" intermediate does not play a significant role in isomerization. However, after heating a solution of [(dmpe)$_2$MnD$_2$(SiH$_2$^{n}Bu)] (**4a**) for three days at 70-80 °C, the Mn*H* and terminal Si*H* signals both achieved 50% deuterium incorporation, suggesting that hydrosilane elimination may be possible at elevated temperatures. Furthermore, hydrosilane exchange reactions were found to occur in the presence of excess free silane, including very slow reactions at room temperature. For example, [(dmpe)$_2$MnH$_2$(SiHPh$_2$)] (**3a**) reacted with ~6 equiv. of PhSiH$_3$ to generate [(dmpe)$_2$MnH$_2$(SiH$_2$Ph)] (**4a**); after three days at room temperature this reaction had proceeded to a 2:1 mixture of **3a**:**4a**, whereas heating overnight at 90 °C afforded complete conversion to **4a**, with no remaining **3a** observed by ^{1}H NMR spectroscopy.[53]

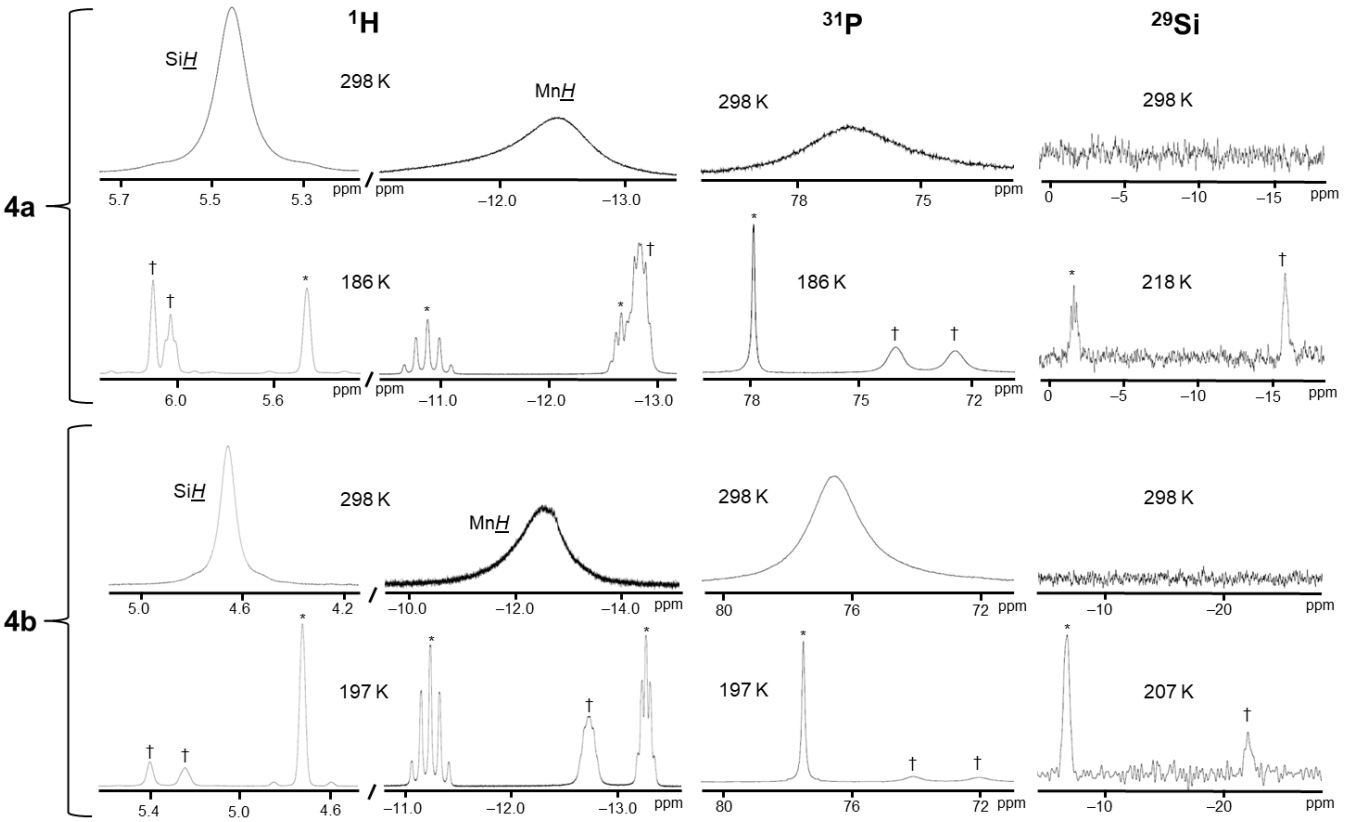

Figure 3. Selected regions of the room temperature and low temperature NMR spectra for (top) [(dmpe)$_2$MnH$_2$(SiH$_2$Ph)] (**4a**) and (bottom) [(dmpe)$_2$MnH$_2$(SiH$_2$^{n}Bu)] (**4b**) showing, from left to right, the silicon hydride and metal hydride regions of the ^{1}H NMR spectra, the ^{31}P{^{1}H} NMR spectra, and ^{29}Si{^{1}H} NMR spectra. Signals in the low temperature spectra are assigned to low symmetry (†; *central*) and high symmetry (*; *transHSi*) isomers.

X-ray Crystal Structures: X-ray quality crystals of **3a**[46] and **4a** (Figure 4; Table 1) were obtained from toluene (**3a**) or hexanes (**4a**) at –30 °C, and in both cases the *central* isomer (the low symmetry isomer observed in solution) was obtained. The geometry at manganese can be described as capped octahedral, with the four phosphorus donors and two *cis*-hydride ligands at the points of a distorted octahedron, and the silyl ligand positioned close to the H–H edge; nearly equidistant from the two hydride ligands, but with a 30.4-37.6° angle between the H(1A)–Si–H(1B) and H(1A)–Mn–H(1B) planes. The Si–H(1A) and Si–H(1B) distances of 1.75(4)-1.79(2) Å in **3a** and 1.77(4)-1.82(3) Å in **4a** are suggestive of significant H–Si interactions, consistent with an η^3-coordinated silicate ($H_2SiR_3^-$) ligand. Crystallographically well-characterized monometallic examples of *central* η^3-H_2SiR_3 ligand systems have been reported for Fe,[18] Co,[41] Mo,[44] Rh,[43] and Ru,[15,19,22,40,42,45] and exhibit Si–H distances ranging from 1.69(3) to 2.15 Å, encompassing the values observed in **3a** and **4a**. As in these literature examples, the substituents on silicon in **3a** and **4a** form a distorted square pyramid with both μ-H atoms in the square plane.

By contrast, crystallization of **4b** from hexanes at –30 °C afforded a structure (a in Figure 5) consistent with the *transHSi* isomer (the high symmetry isomer observed in solution). The geometry at manganese can be described as octahedral, with a hydride ligand coordinated *trans* to a hydrosilane ligand. Unfortunately, four-fold disorder of the silicon moiety prevented location of the three hydrogen atoms bound to Si (two terminal on Si and one bridging between Si and Mn) from the

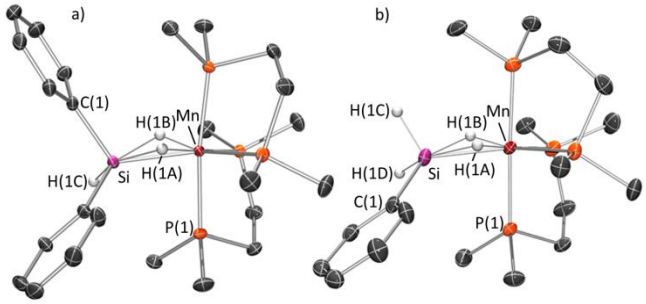

Figure 4. X-ray crystal structures of (a) the *central* isomer of [(dmpe)$_2$MnH$_2$(SiHPh$_2$)] (***central*-3a**),[46] and (b) the *central* isomer of [(dmpe)$_2$MnH$_2$(SiH$_2$Ph)] (***central*-4a**). Ellipsoids are drawn at 50% probability. Hydrogen atoms on Mn and Si were located from the difference map and refined isotropically. All other hydrogen atoms have been omitted for clarity. Bond distances (Å) and angles (deg) for ***central*-4a**: Mn(1)–Si(1) 2.3148(8), Mn(1)–H(1A) 1.49(3), Mn(1)–H(1B) 1.54(3), Si(1)–H(1A) 1.82(3), Si(1)–H(1B) 1.77(4), Si(1)–H(1C) 1.44(3), Si(1)–H(1D) 1.48(3), Mn(1)–Si(1)–C(1) 120.48(9), H(1A)–Mn(1)–Si(1) 52(1), H(1B)–Mn(1)–Si(1) 50(1), H(1A)–Mn(1)–H(1B) 97(2).

difference map. However, DFT calculations on a model of ***transHSi*-4b** where the ^{n}Bu group has been replaced by an Et group (***transHSi*-4b***) afforded a structure with very similar placement of the terminal manganese hydride ligand and the heavy atoms around Mn and Si (b in Figure 5): the calculated Mn–Si distance is 2.36 Å (cf. 2.388(3) Å in the X-ray structure), and the Mn–Si–C(1) and Si–Mn–H(1) angles are 121.8° and

162.3° (cf. 121.8(3)° and 163.0(6)°, respectively, in the X-ray structure).[54] The calculated structure of ***transHSi*-4b*** also features two terminal Si–H bonds (Si–H = 1.52 Å) accompanied by one hydrogen atom (H_{MnSi}) bridging between Mn and Si, with bond lengths and angles (Si–H_{MnSi} = 1.79 Å; Mn–H_{MnSi} = 1.56 Å; Mn–H_{MnSi}–Si = 49.2°) suggestive of a nonclassical hydrosilane ligand; the result of incomplete hydrosilane oxidative addition. Other crystallographically characterized monometallic complexes featuring a nonclassical η^2-(Si–H)-coordinated hydrosilane ligand accompanied by at least one noninteracting metal hydride ligand have been reported for Fe,[55] Nb,[13] Mo,[44] W,[56] and Ru.[14,15,20,23,24,57,58]

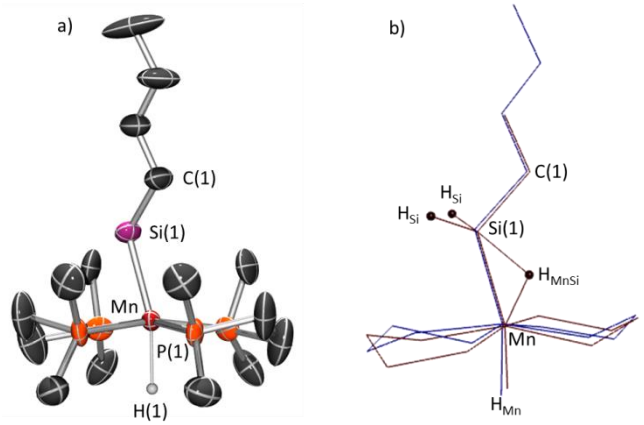

Figure 5. a) X-ray crystal structure of the *transHSi* isomer of [(dmpe)$_2$MnH$_2$(SiH$_2$^{n}Bu)] (***transHSi*-4b**) with ellipsoids drawn at 50% probability. The terminal metal hydride atom was located from the difference map and refined isotropically. All other hydrogen atoms have been omitted for clarity. The Si atom is disordered over 4 positions (2 sets of 2 related by symmetry), the butyl group is disordered over 2 positions (related by symmetry), and the dmpe ligands are disordered over 8 positions (4 sets of 2 related by symmetry). Only one conformation is shown for clarity, with occupancies of 36.8(3)% and 16.0(1)% for silicon and the dmpe ligands, respectively. Bond distances (Å) and angles (deg), where Si(1A) is the Si position that is not shown in the depicted conformation: Mn(1)–Si(1) 2.388(3), Mn(1)–Si(1A) 2.386(3), Mn(1)–H(1) 1.75(5), Mn(1)–Si(1)–C(1) 121.8(3), Mn(1)–Si(1A)–C(1) 127.8, H(1)–Mn(1)–Si(1) 163.0(7), H(1)–Mn(1)–Si(1A) 158(1). b) Overlay of the X-ray crystal structure (blue) of [(dmpe)$_2$MnH$_2$(SiH$_2$^{n}Bu)] (***transHSi*-4b**) and DFT calculated structure (red) of [(dmpe)$_2$MnH$_2$(SiH$_2$Et)] (***transHSi*-4b***), with selected H atoms in the calculated structure depicted as spheres. Methyl groups on the dmpe ligands, and most hydrogen atoms, have been omitted for clarity.

DFT Calculations: To investigate the nature of Si–H 'interligand' interactions in the *central* and *transHSi* isomers of **3a-b** and **4a-b**, and the thermodynamic stability of alternative isomers (*transH$_2$*, *lateralH$_2$*, and *lateralHSi*; Figure 6), we turned to DFT calculations {ADF, gas-phase, all-electron, PBE, D3-BJ, TZ2P, ZORA; **4b** was modelled as [(dmpe)$_2$MnH$_2$(SiH$_2$Et)] (**4b***), with an ethyl group in place of the ^{n}Bu group}. These calculations yielded energy minima (see Figure 7) corresponding to four sets of isomers; the two experimentally observed isomers (*central* and *transHSi*, with good agreement in the relevant bond lengths and angles; Table 1) and two higher energy isomers: *transH$_2$* and *lateralH$_2$* (Figure 6, Table 1, and for **3b**, Figure 8). However, in no case was an energy minimum located for a *lateralHSi* isomer (Figure 6).

As in the X-ray structures of **3a** and **4a**, the *central* isomers have an octahedral arrangement of the phosphorous and H_{MnSi} atoms, with silicon located approximately between the two bridging H_{MnSi} atoms (the angle between the H_{MnSi1}/Mn/H_{MnSi2} and H_{MnSi1}/Si/H_{MnSi2} planes ranges from 17 to 36°). The *transHSi* isomers feature an approximately octahedral arrangement of the phosphorous donors, H_{Mn}, and an η^2-nonclassical hydrosilane ligand, with H_{Mn} approximately *trans* to the centroid of the Si–H_{MnSi} bond, and the four phosphorous donors distorted away from the nonclassical hydrosilane unit. Similarly, the *transH$_2$* isomer is octahedral with *trans*-disposed dihydrogen and silyl ligands. By contrast, the *lateralH$_2$* isomer features *cis*-disposed H_2 and silyl ligands, with Mn, Si, and both H atoms of the dihydrogen ligand located nearly in a plane. The geometry at manganese is approximately octahedral, although the dihydrogen ligand is displaced in the direction of the neighboring silyl ligand (centroid$_{H2}$–Mn–Si = 79-82°). In all four calculated isomers of **3a-b**, **4a**, and **4b***, the Mn–Si–C angles lie between 114 and 126°, while the Mn–Si–H_{Si} angles range from 111 to 118°.

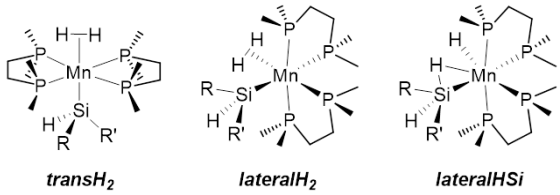

Figure 6. Structures of experimentally unobserved *transH$_2$*, *lateralH$_2$*, and *lateralHSi* isomers of [(dmpe)$_2$MnH$_2$(SiHRR')] (**3a**: R = R' = Ph; **3b**: R = R' = Et; **4a**: R = H, R' = Ph; **4b***: R = H, R' = Et). Of these, energy minima were only located for the *transH$_2$* and *lateralH$_2$* isomers by DFT calculations. For structures of the experimentally observed *central* and *transHSi* isomers (for which energy minima were also located via DFT), see Scheme 2.

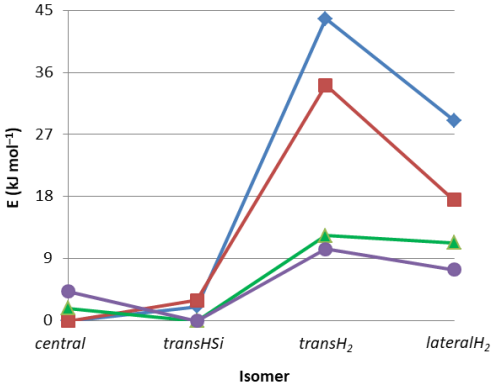

Figure 7. Relative total bonding energies (kJ mol^{-1}) of the *central*, *transHSi*, *transH$_2$*, and *lateralH$_2$* isomers of [(dmpe)$_2$MnH$_2$(SiHPh$_2$)] (**3a**; blue ♦), [(dmpe)$_2$MnH$_2$(SiHEt$_2$)] (**3b**; red ■), [(dmpe)$_2$MnH$_2$(SiH$_2$Ph)] (**4a**; green ▲), and [(dmpe)$_2$MnH$_2$(SiH$_2$Et)] (**4b***; purple ●).

For all complexes (**3a-b**, **4a** and **4b***), the *central* and *transHSi* isomers are within 4 kJ mol^{-1} of each other (Figure 7), consistent with their observation by solution NMR spectroscopy (*vide supra*). In contrast, the two higher energy isomers (*transH$_2$* and *lateralH$_2$*) are 8-44 kJ mol^{-1} higher in energy than the most stable experimentally observed isomer, with a larger energy difference in the case of more sterically hindered **3a** and **3b** (Figure 7). These isomers likely exist in

Table 1. Selected angles (deg) and distances (Å) (and Mayer bond orders) for *central*, *transHSi*, *transH*$_2$, and *lateralH*$_2$ isomers from calculated {or X-ray} structures of **3a-b**, **4a-b**, and **4b***. Atom labels correspond to those for **3b** in Figure 8.

	[(dmpe)$_2$MnH$_2$(SiHRR')]	**3a**	**3b**	**4a**	**4b/4b***
	SiHRR'	$SiHPh_2$	$SiHEt_2$	SiH_2Ph	SiH_2Et {XRD: $SiH_2{}^nBu$}
central isomer	Mn–Si	2.31 (0.63) {2.3176(3)}	2.35 (0.69)	2.31 (0.69) {2.3148(8)}	2.32 (0.69)
	Mn–H_{MnSi}	1.57, 1.59 (0.62, 0.67) {1.46(3), 1.62(3)}	1.56, 1.57 (0.70, 0.71)	1.57, 1.58 (0.66, 0.70) {1.49(3), 1.54(3)}	1.57 (0.68, 0.70)
	Si–H_{MnSi}	1.82, 1.85 (0.28, 0.33) {1.75(4), 1.79(2)}	1.85, 1.88 (0.25, 0.26)	1.84, 1.87 (0.28, 0.29) {1.77(4), 1.82(3)}	1.83, 1.88 (0.27, 0.28)
	Si–H_{Si}	1.52 (0.81) {1.37(4)}	1.51 (0.81)	1.50, 1.51 (0.83, 0.88) {1.44(3), 1.48(3)}	1.51, 1.52 (0.84)
	H_{MnSi}–Mn–Si	51.9, 52.9 {49(1), 50(1)}	52.0, 53.1	52.3, 53.4 {50(1), 52(1)}	51.8, 53.5
	H_{MnSi}–Mn–H_{MnSi}	98.3 {92(2)}	103.8	101.1 {97(2)}	103.0
	Mn–Si–C	116.5, 118.4 {117.65(3), 119.69(3)}	117.5, 120.3	119.6 {120.48(9)}	119.9
	Mn–Si–H_{Si}	116.3 {114(2)}	111.7	114.9, 117.7 {115(1), 120(1)}	113.8, 116.9
	H_{MnSi}/Mn/H_{MnSi} plane to H_{MnSi}/Si/H_{MnSi} plane	36.4 {37.6}	16.6	30.7 {30.4}	22.2
transHSi isomer	Mn–Si	2.36 (0.77)	2.39 (0.71)	2.35 (0.81)	2.36 (0.78) {2.386(3), 2.388(3)}
	Mn–H_{MnSi}	1.57 (0.57)	1.57 (0.64)	1.57 (0.62)	1.56 (0.63)
	Mn–H_{Mn}	1.56 (0.82)	1.57 (0.83)	1.57 (0.80)	1.57 (0.83) {1.75(5)}
	Si–H_{MnSi}	1.80 (0.34)	1.75 (0.33)	1.82 (0.31)	1.79 (0.30)
	Si–H_{Si}	1.52 (0.74)	1.52 (0.80)	1.51, 1.52 (0.79, 0.86)	1.52 (0.81, 0.82)
	H_{MnSi}–Mn–Si	49.6	47.1	50.8	49.2
	H_{Mn}–Mn–Si	162.3	162.4	161.7	162.3 {158(1), 163.0(7)}
	H_{Mn}–Mn–SiH_{MnSi}(centroid)	178.1	178.7	177.2	178.4
	Mn–Si–C	118.3, 119.0	116.2, 118.1	120.0	121.8 {121.8(3), 127.8}
	Mn–Si–H_{Si}	115.6	112.6	115.9, 116.1	114.2, 115.3
transH$_2$ isomer	Mn–Si	2.41 (0.95)	2.41 (0.89)	2.37 (0.96)	2.36 (0.93)
	Mn–H_{Mn}	1.58, 1.59 (0.55)	1.58 (0.61)	1.59 (0.56)	1.59 (0.59, 0.60)
	Si–H_{Mn1}	3.93, 3.96 (<0.05)	3.94, 3.95 (<0.05)	3.91, 3.92 (<0.05)	3.90 (<0.05)
	Si–H_{Si}	1.51 (0.78)	1.52 (0.77)	1.51, 1.52 (0.81)	1.52, 1.53 (0.79, 0.80)
	H_{Mn}–H_{Mn}	0.96 (0.43)	0.99 (0.38)	0.96 (0.44)	0.98 (0.41)
	H_{Mn}–Mn–H_{Mn}	35.3	36.7	35.3	36.1
	H_2(centroid)–Mn–Si	177.0	177.3	175.1	174.2
	Mn–Si–C	122.9, 124.2	120.9, 121.6	123.6	124.8
	Mn–Si–H_{Si}	111.4	113.9	115.0, 115.8	114.8, 115.7
lateralH$_2$ isomer	Mn–Si	2.39 (0.91)	2.40 (0.90)	2.35 (0.91)	2.36 (0.91)
	Mn–H_{Mn1}	1.57 (0.48)	1.56 (0.53)	1.57 (0.51)	1.57 (0.53)
	Mn–H_{Mn2}	1.59 (0.62)	1.59 (0.63)	1.59 (0.62)	1.59 (0.62)
	Si–H_{Mn1}	2.17 (0.12)	2.12 (0.13)	2.16 (0.14)	2.13 (0.14)
	Si–H_{Mn2}	3.05 (<0.05)	3.03 (<0.05)	3.07 (<0.05)	3.04 (<0.05)
	Si–H_{Si}	1.52 (0.76)	1.53 (0.76)	1.52 (0.79, 0.82)	1.52, 1.53 (0.80, 0.81)
	H_{Mn1}–H_{Mn2}	0.99 (0.40)	1.00 (0.39)	1.01 (0.41)	1.00 (0.41)
	H_{Mn1}–Mn–Si	62.6	60.6	63.5	62.1
	H_{Mn1}–Mn–H_{Mn2}	36.6	36.8	37.2	37.0
	H_2(centroid)–Mn–Si	80.4	79.0	82.2	80.7
	Mn–Si–C_1	117.1	113.8	120.8	119.4
	Mn–Si–C_2	125.9	123.6	–	–
	Mn–Si–H_{Si}	113.9	113.2	115.8, 116.7	116.2
	H_{Mn1}–Mn–Si–C_1	19.5	5.5	–12.0	0.5
	H_{Mn1}–Mn–Si–C_2	–103.4	–118.6	–	–
	H_{Mn1}–Mn–Si–H_{Si}	135.0	121.1	111.3, –131.3	121.6, –121.0

equilibrium with the experimentally observed isomers, but in concentrations too low for NMR spectroscopic observation. In fact, a *transH*$_2$ or *lateralH*$_2$ isomer is presumably formed initially in the synthesis of **3a-b** and **4a-b** via the reactions of H_2 with silylene hydride complexes **1a-b** or disilyl hydride complexes **2a-b** (*vide supra*).

Both experimentally observed isomers (*central* and *transHSi*) feature nonclassical bonding situations. This is apparent from Mayer bond orders of 0.25-0.34 between silicon and the bridging hydride ligands (Si–H_{MnSi}), as well as Mn–Si Mayer bond orders ranging from 0.63 to 0.81 (cf. 0.89 to 0.96 for the *transH*$_2$ and *lateralH*$_2$ isomers, which feature silyl ligands without strong interactions to neighboring hydride ligands; *vide infra*).

The *transHSi* isomers can simply be described as nonclassical hydrosilane complexes; structures intermediate between σ-hydrosilane and classical silyl hydride extremes, as a consequence of substantial but incomplete Si–H bond oxidative addition. By contrast, the similar Si–H_{MnSi} and Mn–H_{MnSi} Mayer bond orders involving both H_{MnSi} atoms in the *central* isomers are indicative of a nonclassical η^3-H_2SiHRR' (silicate) anion.[59]

In contrast to the nonclassical *central* and *transHSi* isomers, the *transH*$_2$ and *lateralH*$_2$ isomers can be described as silyl η^2-H_2 complexes. These isomers feature significant H–H interactions, reflected by H–H distances of 0.96-1.01 Å (relative to 0.75 Å for free H_2), Mayer H–H bond orders of 0.38-0.44, and acute H–Mn–H angles of 35.3-37.2° (Table 1). Nevertheless, the *lateralH*$_2$ isomer of **3a-b**, **4a**, and **4b*** features small but non-negligible Si–H_{Mn1} Mayer bond orders (0.12-0.14), a Mn–H_{Mn1} Mayer bond order which is 0.09-0.14 lower than that of Mn–H_{Mn2}, as well as acute (79-82°) angles between the centroid of the H_2 ligand, Mn and Si (Table 1). These features suggest a minor degree of bonding between Si and H_{Mn1}, and the lower extent of Si–H_{Mn1} bonding in the *lateralH*$_2$ versus the *central* or *transHSi* isomers is also reflected in Si–Mn–H_{Mn1} angles of 60.6-63.5° in the former, which are much more obtuse than the corresponding Si–Mn–H angles in the latter (*central*; 51.8-53.5°, *transHSi*; 47.1-50.8°).

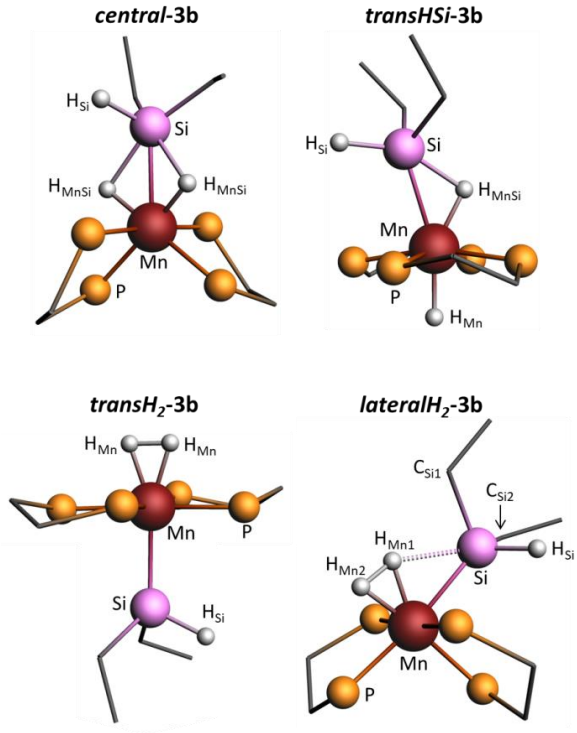

Figure 8. Geometry optimized structures of the isomers of [(dmpe)$_2$MnH$_2$(SiHEt$_2$)] (**3b**) determined by DFT calculations. Spheres represent Mn (red), Si (pink), P (orange), and H (white), whereas carbon atoms are represented by grey vertices. *P*-methyl groups and most H atoms have been omitted for clarity.

The lack of substantial interligand Si–H interactions in the *lateralH*$_2$ isomers lies in contrast to the literature on transition metal complexes with a meridional Si–H–H arrangement of SiR_3 and H moieties, which suggests that complexes featuring a hydrosilane and a hydride ligand (i.e. the proposed *lateralHSi* isomer in Figure 6) should typically be favored relative to a silyl dihydrogen complex (i.e. the *lateralH*$_2$ isomer).[13,20,24] Such a preference has been rationalized[60] based primarily on H–H and Si–H bond strengths.[61] In this work, the expected trend is reflected in the experimental observation of the *transHSi* isomer of **3a-b** and **4a-b** but not the *transH*$_2$ isomer.

Our inability to locate an energy minimum for a *lateralHSi* isomer (*vide supra*) was surprising, and prompted us to investigate sterically less encumbered PH_3 analogues of **3a-b** and **4a-b**; ([$(PH_3)_4MnH_2$(SiHRR')]: **3a^{PH3}**; R = R' = Ph, **3b^{PH3}**; R = R' = Et, **4a^{PH3}**; R =H, R' = Ph, and **4b^{PH3}**; R = H, R' = Et). These calculations afforded energy minima corresponding to the four previously calculated isomers (*central*, *transHSi*, *transH*$_2$, and *lateralHSi*), as well as a *lateralHSi* isomer (relative energies are plotted in Figure 9). In all cases these *lateralHSi* isomers were lower in energy than the *lateralH*$_2$ isomers, and feature a significant Si–H_{Mn1} interaction (Si–H_{Mn1} dist. 1.88-1.93 Å, Mayer bond order 0.25-0.32, Si–Mn–H_{Mn1} angle 51.3-54.0°) and minimal H_{Mn1}–H_{Mn2} interactions (H–H dist. 1.57-1.63 Å, Mayer bond order 0.05-0.08, H_{Mn1}–Mn–H_{Mn2} angle 60.7-63.4°), consistent with *cis*-disposed hydride and nonclassical hydrosilane ligands. Computational observation of the *lateralHSi* isomers for the PH_3 analogues, but not the dmpe complexes, suggests that the *lateralHSi* isomers are sterically disfavored in the dmpe complexes.[62]

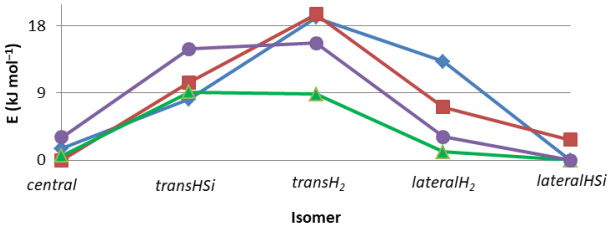

Figure 9. Relative total bonding energies (kJ mol^{-1}) of the *central*, *transHSi*, *transH*$_2$, *lateralH*$_2$, and *lateralHSi* isomers of silyl dihydride complexes where the two dmpe ligands have been replaced with four PH_3 ligands; [$(PH_3)_4MnH_2$(SiHPh$_2$)] (**3a^{PH3}**; blue ♦), [$(PH_3)_4MnH_2$(SiHEt$_2$)] (**3b^{PH3}**; red ■), [$(PH_3)_4MnH_2$(SiH$_2$Ph)] (**4a^{PH3}**; green ▲), and [$(PH_3)_4MnH_2$(SiH$_2$Et)] (**4b^{PH3}**; purple ●).

Determination of Sign and Magnitude of $J_{Si,H}$: As noted previously, the ^{29}Si–^{1}H coupling constant ($J_{Si,H}$) can provide a sensitive experimental measure of where a structure lies along the continuum from a σ-hydrosilane complex to a classical silyl hydride complex. However, this requires knowledge of both the magnitude and sign of $J_{Si,H}$ (*vide supra*).

Scherer has used standard 2D ^{1}H–^{1}H COSY NMR spectroscopy to unambiguously determine the sign of $J_{Si,H}$ in transition metal silyl hydride/hydrosilane complexes; specifically, those where silicon bears at least one terminal hydrogen substituent.[27,28] This method takes advantage of passive coupling; coupling which is not directly responsible for the formation of a particular cross-peak.[63] For example, in an AMX spin system (A and M are proton environments, and X is a spin ½ nucleus) where active A–M coupling gives rise to a ^{1}H–^{1}H COSY cross-peak, passive A–X and M–X coupling results in additional splitting of the cross-peak into a doublet where a diagonal line can be drawn between the two peaks which compose the doublet; the slope of which can be used to determine the relative sign of the two passive coupling constants (J_{XA} and J_{XM}).[63]

In Scherer's experiment, this involves measurement of the vector between ^{29}Si satellites of a ^{1}H–^{1}H COSY cross-peak between a terminal Si*H* signal (H_{Si}) and a metal-coordinated hydride signal (H_M).[27,28] If the slope of this vector is positive, then the two passive $J_{Si,H}$ couplings ($J_{Si,H}$ to H_M, *the sign of which is unknown*, and $^{1}J_{Si,H}$ to H_{Si}, *which is known to be*

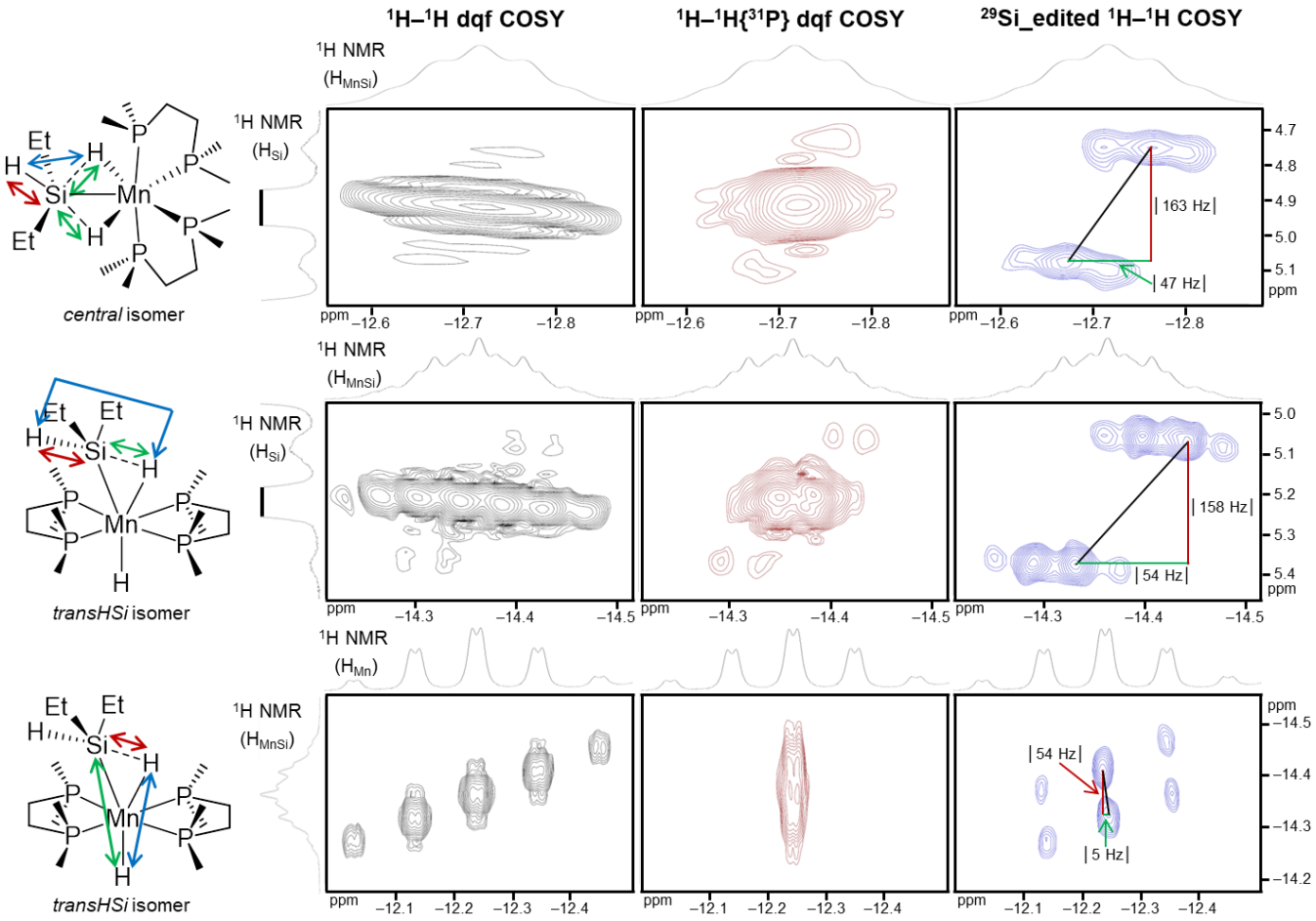

Figure 10. Comparisons of $^{1}H–^{1}H$ COSY spectra (500 MHz, d_8-toluene) of [(dmpe)$_2$MnH$_2$(SiHEt$_2$)] (**3b**) at 229 K showing cross-peaks (with ^{29}Si satellites) used to measure the sign and magnitude of $J_{Si,H}$ via coupling between (top row) *central* isomer H_{Si} and H_{MnSi} environments, (middle row) *transHSi* isomer H_{Si} and H_{MnSi} environments, and (bottom row) *transHSi* isomer H_{MnSi} and H_{Mn} environments. From left to right within a row, the same spectral regions are shown with equivalent acquisition parameters (e.g. ns, td1eff: Table S1) in the standard $^{1}H–^{1}H$ dqf COSY spectrum (black), the $^{1}H–^{1}H\{^{31}P\}$ dqf COSY spectrum (red), and the ^{29}Si_edited $^{1}H–^{1}H$ COSY spectrum (blue). Peak labels match those in Figure 8. In the structures to the left of each row, the blue arrow indicates the two ^{1}H environments whose active coupling gives rise to the cross-peak shown, the red arrow indicates the passive $^{1}H–^{29}Si$ coupling used as an internal reference in the measurement, and the green arrow indicates the passive $^{1}H–^{29}Si$ coupling being measured. The lines on the cross-peaks in the ^{29}Si_edited $^{1}H–^{1}H$ COSY spectra represent the vector between the ^{29}Si satellites (black line; used to determine relative sign), the magnitude of the coupling used as the internal reference (red line), and the magnitude of $J_{Si,H}$ for which the sign is being determined (green line).

negative[34]) have the same sign, so $J_{Si,H}$ to H_M is negative. By contrast, if the slope is negative, the two passive $J_{Si,H}$ couplings have opposite signs, and $J_{Si,H}$ to H_M is positive; $^{1}J_{Si,H}$ coupling to the terminal Si*H* proton (H_{Si}) therefore serves as an internal reference.[27,28] The magnitudes of the two passive $J_{Si,H}$ couplings can also be measured directly from the 2D $^{1}H–^{1}H$ COSY NMR spectrum, since the horizontal and vertical distances between the ^{29}Si satellites provide the magnitudes of $J_{Si,H}$ to H_M and H_{Si}.

However, for **3a-b** and **4a-b**, we had difficulty obtaining standard $^{1}H–^{1}H$ dqf COSY NMR spectra with well-defined ^{29}Si satellites (Figure 10); in some cases the signal could not be detected from the noise, while in others the signals were too broad for accurate measurement, or could not be resolved from the parent cross-peak. In an effort to more clearly resolve the ^{29}Si satellites of the COSY NMR cross-peaks, two modifications of a standard 2D COSY experiment were investigated. One modification involved applying broadband ^{31}P decoupling during FID acquisition of a dqf COSY $^{1}H–^{1}H$ NMR experiment (a 2D $^{1}H–^{1}H\{^{31}P\}$ dqf COSY NMR experiment), as a means to increase the signal/noise and improve resolution of the cross-peaks by concentrating the signal (which is spread into a multiplet by coupling to four ^{31}P atoms) over a smaller area. The second modification was ^{29}Si editing to filter out all of the signal which is not interacting with ^{29}Si. This 2D ^{29}Si_edited $^{1}H–^{1}H$ COSY NMR experiment eliminates the parent cross-peak (which contains 95% of the intensity), allowing ^{29}Si satellites which overlap with the parent cross-peak to be resolved. Furthermore, it increases the signal-to-noise for the ^{29}Si satellites by removing unnecessary signal, allowing for a much higher receiver gain.

Figure 10 shows a comparison of the cross-peaks required to measure the sign of $J_{Si,H}$ for various protons in $^{1}H–^{1}H$ dqf COSY, $^{1}H–^{1}H\{^{31}P\}$ dqf COSY, and ^{29}Si_edited $^{1}H–^{1}H$ COSY NMR spectra for the two experimentally observed isomers of [(dmpe)$_2$MnH$_2$(SiHEt$_2$)] (**3b**) at 229 K. These experiments used the same NMR sample, the same number of scans, and identical td1eff values (leading to nearly identical experiment times; Table S1), and it can be seen that the $^{1}H–^{1}H\{^{31}P\}$ dqf COSY experiment provided only a marginal improvement in resolution

relative to a standard ^{1}H–^{1}H dqf COSY spectrum; likely because decoupling was only possible in the direct dimension, so the signal remained spread out in the indirect dimension (the y-axis). By contrast, the ^{29}Si_edited ^{1}H–^{1}H COSY experiment provided substantially more intense ^{29}Si satellites and allowed for more accurate identification of ^{29}Si satellite peak positions, as well as observation of satellites buried under the parent cross-peak in the standard ^{1}H–^{1}H dqf COSY spectrum. Therefore, all further discussion focuses on the results of ^{29}Si_edited ^{1}H–^{1}H COSY experiments.

The top row of Figure 10 shows the cross-peak, in ***central*-3b**, between the terminal Si*H* proton (H_{Si}) and the hydride ligands bridging between Si and Mn (2 x H_{MnSi}; equivalent on the NMR timescale). The middle row of Figure 10 shows the cross-peak, in ***transHSi*-3b**, between the terminal Si*H* proton (H_{Si}) and the single hydride bridging between Si and Mn (H_{MnSi}). The positive slope of the line between the ^{29}Si satellites on both of these cross-peaks is indicative of negative $J_{Si,H}$ values for the H_{MnSi} protons in ***central*-3b** and ***transHSi*-3b** (–47 and –54 Hz, respectively). By contrast, the bottom row of Figure 10 shows the cross-peak between H_{MnSi} and the terminal hydride ligand, H_{Mn}, in ***transHSi*-3b**. In this case, because $J_{Si,H}$ has been determined to be negative for H_{MnSi} in ***transHSi*-3b** (*vide supra*), the negative slope of the line between the ^{29}Si satellites indicates that $J_{Si,H}$ for H_{Mn} in ***transHSi*-3b** is positive (5 Hz), as expected for a 2-bond ^{29}Si–^{1}H coupling.

Analogous trends were observed for the *central* and *transHSi* isomers of **3a** and **4a-b** (Figures S3-S6 and Table 2). However, we were unable to observe coupling constants from particularly weak cross-peaks, precluding determination of the sign of $J_{Si,H}$ for H_{MnSi} in the *central* isomers of **3a** and **4b** or for H_{Mn} in the *transHSi* isomer of **3a** (present as a minor isomer; 13%). DFT-calculated coupling constants are also provided in Table 2, and are in good agreement with those determined experimentally.

Table 2. ^{29}Si–H coupling constants ($J_{Si,H}$) measured by ^{29}Si_edited ^{1}H–^{1}H COSY NMR spectroscopy (and calculated by DFT) for complexes **3a-b**, **4a-b**, and **4b*** (Hz).

Complex	**3a**	**3b**	**4a**	**4b/4b***
Silyl group	$SiHPh_2$	$SiHEt_2$	SiH_2Ph	$SiH_2{}^nBu$[a]
$J_{Si,H}$ for H_{MnSi} in the *central* isomer	n.o.[b] (–45, –49)	–47 (–35, –45)	<0[c] (–41, –44)	n.o.[b] (–38, –43)
$J_{Si,H}$ for H_{MnSi} in the *transHSi* isomer	–41 (–38)	–54 (–47)	–38 (–26)	–43 (–33)
$J_{Si,H}$ for H_{Mn} in the *transHSi* isomer	n.o.[b] (13)	5 (12)	9 (13)	9 (14)

(a) In the calculated complex, **4b***, the silyl group is SiH_2Et. (b) n.o. = not observed. (c) This cross-peak was too broad to accurately measure.

For the *central* isomer of **3b**, the $J_{Si,H}$ coupling constant for H_{MnSi} is –47 Hz, and the average calculated values for **3a-b** and **4a-b** range from –40 to –47 Hz. Literature values of $J_{Si,H}$ for H_{MnSi} in η^3-coordinated silicate ($H_2SiR_3^-$) complexes typically range in magnitude from 11 to 54 Hz.[15,18,19,42,43,45] To the best of our knowledge, the sign of $J_{Si,H}$ has not been experimentally determined for these literature complexes, but calculations have, in at least one case, been performed and indicate a negative sign.[18] Assuming that all of these $J_{Si,H}$ values are negative, the $J_{Si,H}$ coupling constants for H_{MnSi} in **3a-b** and **4a-b** lie towards the more negative end of the reported range, indicative of non-classical silicate complexes with relatively strong Si– H_{MnSi} interactions.

For the *transHSi* isomer of **3a-b** and **4a-b**, the $J_{Si,H}$ coupling constants for H_{MnSi} range from –38 to –54 Hz (calcd. –26 to –47 Hz), falling within the region typically associated with non-classical hydrosilane complexes (0 to –70 Hz; *vide infra*), indicative of partial oxidative addition of the Si–H_{MnSi} bond. Using both experimental and calculated values, two clear trends can be observed in $J_{Si,H}$ for H_{MnSi} in the *transHSi* isomers; more negative $J_{Si,H}$ coupling constants were seen for aliphatic versus aromatic analogues, and for disubstituted versus monosubstituted analogues. This trend appears to reflect the trend in bond metrics (*vide supra*), for which stronger Si–H interactions in aliphatic and disubstituted analogues (relative to aromatic and monosubstituted analogues respectively) were calculated. The former can be rationalized based on a larger degree of π back-donation to hydrosilanes with aryl substituents, whereas the latter is presumably steric in origin, with disubstituted hydrosilanes decreasing the extent of Si–H bond oxidative addition.

SUMMARY AND CONCLUSIONS

Silyl dihydride complexes of manganese, **3a-b** and **4a-b**, were synthesized via the reactions of H_2 with silylene hydride (**1a-b**) and disilyl hydride (**2a-b**) complexes. These reactions suggest that both **1a-b** and **2a-b** exist in equilibrium with a shared low-coordinate silyl species, "$(dmpe)_2Mn(SiH_{3-x}R_x)$", accessed via 1,1-insertion from **1a-b**, and hydrosilane reductive elimination from **2a-b**.

Complexes **3a-b** and **4a-b** provide an uncommon opportunity to study silyl dihydride complexes differing in the number (1 vs 2) and nature (aromatic vs alkyl) of the hydrocarbyl substituents on silicon. In solution, **3a-b** and **4a-b** exist as an equilibrium mixture of a *central* isomer featuring a meridional H–Si–H arrangement of the silyl and hydride ligands, and a *transHSi* isomer with *trans*-disposed hydrosilane and hydride ligands. These isomers contain a single silicon center involved in either one or two Si–H–Mn bridging interactions, and combined XRD, DFT, and NMR spectroscopic studies indicate that the *central* and *transHSi* isomers can be considered to contain a nonclassical silicate (η^3-H_2SiR_3) anion, and a nonclassical hydrosilane ligand, respectively. Additionally, DFT calculations indicate the thermodynamic accessibility of *lateralH*$_2$ and *transH*$_2$ isomers with *cis*- and *trans*-disposed silyl and dihydrogen ligands, respectively (these isomers may be present in solution at concentrations below that detectable by NMR spectroscopy). Furthermore, a *lateralHSi* isomer featuring *cis*-disposed hydride and nonclassical hydrosilane ligands was observed in DFT calculations on sterically-minimized PH_3 analogues of **3a-b** and **4a-b**.

Measurement of the sign and magnitude of $J_{Si,H}$ in the *central* and *lateralHSi* isomers of **3a-b** and **4a-b** was made possible using a modification of Scherer's method, employing 2D ^{1}H–^{1}H COSY NMR spectroscopy with ^{29}Si editing to remove all of the signal which is not interacting with ^{29}Si. This ^{29}Si_edited ^{1}H–^{1}H COSY experiment allowed accurate location of ^{29}Si satellites which were unobserved in 'standard' ^{1}H–^{1}H dqf COSY experiments. Additionally, it allowed determination of small $J_{Si,H}$ couplings (e.g. 5 Hz) where the pertinent signals are broadened by ^{31}P coupling; previous methods used to determine the magnitude of similar couplings relied upon experiments requiring non-standard NMR probes which can simultaneously be tuned to ^{29}Si and ^{31}P (e.g. ^{29}Si{^{31}P} INEPT[64] and ^{29}Si–^{1}H–{^{31}P} HMQC[65] experiments). By contrast, the ^{29}Si_edited ^{1}H–^{1}H COSY experiment used in this report can be run on a standard double resonance NMR probe with a single broadband channel.

The utility of the ^{29}Si_edited ^{1}H–^{1}H COSY NMR experiment was also highlighted by measurement of the sign and magnitude of $J_{Si,H}$ for H_{MnSi} in the nonclassical disilyl hydride complexes [(dmpe)$_2$MnH(SiH$_2$R)$_2$] (**2a**: R = Ph, **2b**: R = ^{n}Bu). These experiments (Figures S1-S2) afforded coupling constants of –31 Hz (**2a**) and –30 Hz (**2b**), which are in good agreement with the calculated values of –24 and –27 Hz, respectively, in our initial report,[66] and provide further experimental support for the nonclassical bonding situation proposed in **2a-b** (significant interactions between the central hydride and both flanking silyl groups).

EXPERIMENTAL SECTION

General Details. An argon-filled MBraun UNIlab glove box equipped with a –30 °C freezer was employed for the manipulation and storage of all oxygen- and moisture- sensitive compounds. Air-sensitive preparative reactions were performed on a double-manifold high-vacuum line equipped with a two stage Welch 1402 belt-drive vacuum pump (ultimate pressure 1×10^{-4} torr) using standard techniques.[67] The vacuum was measured periodically using a Kurt J. Lesker 275i convection enhanced Pirani gauge. Commonly utilized specialty glassware included thick walled flasks equipped with Teflon stopcocks, and J-Young or Wilmad-LabGlass LPV NMR tubes. Residual oxygen and moisture was removed from the argon stream by passage through an Oxisorb-W scrubber from Matheson Gas Products.

Benzene and hexamethyldisiloxane were purchased from Aldrich, hexanes was purchased from Caledon, and deuterated solvents were purchased from ACP Chemicals. Benzene, hexamethyldisiloxane, and hexanes were initially dried and distilled at atmospheric pressure from sodium/benzophenone. All solvents were stored over an appropriate drying agent (hexamethyldisiloxane, benzene, d^8 toluene, C$_6$D$_6$ = Na/Ph$_2$CO; hexanes = Na/Ph$_2$CO/tetraglyme) and introduced to reactions or solvent storage flasks via vacuum transfer with condensation at –78 °C.

Dmpe, PhSiH$_3$, ^{n}BuSiH$_3$, Ph$_2$SiH$_2$, Et$_2$SiH$_2$, 1,4-dioxane, D$_2$, and ethylmagnesium chloride solution (2.0 M in diethyl ether) were purchased from Sigma-Aldrich. Manganese dichloride was purchased from Strem Chemicals. Argon and hydrogen gas were purchased from PraxAir. [(dmpe)$_2$MnH(=SiR$_2$)] (**1a**: R = Ph, **1b**: R = Et),[46] [(dmpe)$_2$MnH(SiH$_2$R)$_2$] (**2a**: R = Ph, **2b**: R = ^{n}Bu),[47] [(dmpe)$_2$MnH$_2$(SiHR$_2$)] (**3a**: R = Ph, **3b**: R = Et),[46] and [(dmpe)$_2$MnD$_2$(SiHEt$_2$)] (**3b_d$_2$**)[46] were prepared according to the literature. A complete list of NMR data for **3a-b** and **3b_d$_2$** can also be found in the ESI of our previous communication.[46]

NMR spectroscopy was performed on Bruker AV-500 and AV-600 spectrometers. Spectra were obtained at 298 K unless otherwise indicated. All ^{1}H NMR spectra were referenced relative to SiMe$_4$ through a resonance of the protio impurity of the solvent used: C$_6$D$_6$ (δ 7.16 ppm) and d^8 toluene (δ 2.08 ppm, 6.97 ppm, 7.01 ppm, and 7.09 ppm). Also, all ^{13}C NMR spectra were referenced relative to SiMe$_4$ through a resonance of the ^{13}C in the solvents: C$_6$D$_6$ (δ 128.06 ppm) and d^8 toluene (δ 20.43, 125.13, 127.96, 128.87, and 137.48 ppm). The ^{29}Si NMR spectra were referenced using an external standard of hexamethyldisiloxane in CDCl$_3$ (6.53 ppm), and the ^{31}P NMR spectra were referenced using an external standard of 85% H$_3$PO$_4$ in D$_2$O (0.0 ppm).

^{1}H–^{1}H COSY NMR spectra (and variations thereof) used to measure $J_{Si,H}$ were performed on Bruker AV-500 instruments at the warmest temperatures where all peaks are completely resolved. Spectral widths were chosen to ensure all peaks were encompassed. ^{1}H–^{1}H{^{31}P} dqf COSY NMR spectroscopy required input of a ^{31}P chemical shift to be used in calculating the frequency used for ^{31}P decoupling; 75 ppm was used for all samples because it was close to the ^{31}P chemical shifts observed for these complexes. ^{29}Si_edited ^{1}H–^{1}H COSY NMR spectroscopy required input of a transmitter frequency for the pulses on ^{29}Si (calculated from the ^{29}Si chemical shifts; δ_{Si}) and an estimated $J_{Si,H}$ used to calculated the delay required to preferentially select, by polarization transfer, those protons interacting with ^{29}Si (excluding all others). The former was chosen separately for each complex based on an average of the chemical shifts of the *central* and *transHSi* isomers. Determination of the latter involved starting with a 'best guess' determined from 1D ^{1}H NMR spectra (usually the coupling constant between ^{29}Si and a terminal Si*H* proton), followed by repeatedly collecting a 1D slice of a ^{1}H–^{29}Si HSQC experiment varying in estimated $J_{Si,H}$, with the value leading to the greatest intensity of the cross-peak of interest being chosen for use in the 2D experiment. Pertinent parameters (optimized for each sample based on values which gave the best results for ^{29}Si_edited ^{1}H–^{1}H COSY NMR experiments) used for all three COSY-type experiments (number of scans, experiment time, td1eff, td2eff, temperature, and for ^{29}Si_edited ^{1}H–^{1}H COSY only, δ_{Si} and estimated $J_{Si,H}$) are available in the ESI, as are symbolic pulse sequences used for ^{1}H–^{1}H{^{31}P} dqf COSY and ^{29}Si_edited ^{1}H–^{1}H COSY NMR experiments. For all COSY experiments, pulsed field gradients were used for coherence selection and artifact suppression.

Combustion elemental analyses were performed by Midwest Microlabs in Indianapolis, USA. IR spectra were performed in transmission mode on a Bruker Tensor 27 IR spectrometer as a suspension in Nujol or solution in hexanes, in both cases using CaF_2 plates.

All calculated structures were fully optimized with the ADF DFT package (SCM, versions 2014.05 to 2017.207).[68] Calculations were conducted in the gas phase within the generalized gradient approximation using the 1996 Perdew-Burke-Ernzerhof exchange and correlation functional (PBE),[69] using the scalar zeroth-order approximation (ZORA)[70] for relativistic effects, and Grimme's DFT-D3-BJ dispersion correction.[71] To locate global energy minima, various (between 2 and 4) calculations were run for each structure starting from input coordinates associated with all possible rotamers; structures discussed in this work correspond to the lowest of the resultant energy minima in each case. Preliminary geometry optimizations were conducted with frozen cores corresponding to the configuration of the preceding noble gas (core = medium) using double-ζ basis sets with one polarization function (DZP), a Voronoi grid with an integration value of 5, and default convergence criteria for energy and gradients. These structures were further refined using all-electron triple-ζ basis sets with two polarization functions (TZ2P) and fine integration grids (Voronoi 7 or Becke[72] verygood-quality).

Bond orders were calculated within the Mayer[73] formalism. Visualization of the computational results was performed using the ADF-GUI (SCM) or Biovia Discovery Studio Visualizer.

Analytical frequency calculations[74] were conducted on all geometry optimized structures (including geometry optimized fragments) to ensure that the geometry optimization led to an energy minimum and to obtain thermodynamic parameters. In a handful of cases, slightly negative frequencies (frequency range from –10 to –25 cm^{-1}) were observed but were shown to be spurious imaginary frequencies using the SCANFREQ command.[75] In one case (***transH$_2$*-3a**), the observed negative frequency (–9 cm^{-1}) was determined to be a dirty mode caused by low barrier rotation of the Mn–Si bond.

NMR coupling constants were calculated (using geometry optimized coordinates derived as discussed above) with the CPL program of the ADF package[76] from wave functions obtained by hybrid PBE0[77] (ZORA)[70] calculations using the TZ2P basis sets with additional steep basis functions (TZ2P-J). This method was benchmarked against published data calculated for related nonclassical hydrosilane complexes. The literature results[28] were reproduced with acceptable accuracy for [(C$_5$H$_4$Me)MnH(SiHPh$_2$)(CO)$_2$] (our method: –52 Hz, literature calcd.: –68 Hz, literature expt.: –63 Hz[28]), [Cp$_2$TiH(SiHPh$_2$)(PMe$_3$)] (our method: –22 Hz, literature calcd.: –28 Hz, literature expt.: |28| Hz[78]), and [Cp$_2$TiH(SiHClPh)(PMe$_3$)] (our method: 19 Hz, literature calcd.: 23 Hz, literature expt.: 15 Hz[27]).

All reported computational values in this work were derived from restricted calculations (for modeling diamagnetic structures). For the five isomers of **4b^{PH3}**, two additional sets of calculations were conducted to model potential paramagnetic structures using the UNRESTRICTED command[79] in conjunction with forcing two or four unpaired electrons (using the CHARGE command) and explicit occupation numbers (using the OCCUPATIONS command), in each case resulting minima were >180 kJmol^{-1} greater in energy than the corresponding diamagnetic structure.

Single-crystal X-ray crystallographic analyses were performed on crystals coated in Paratone oil and mounted on a Bruker SMART APEX II diffractometer with a 3 kW sealed-tube Mo generator and SMART6000 CCD detector in the McMaster Analytical X-Ray Diffraction Facility (MAX). A semi-empirical absorption correction was applied using redundant data. Raw data was processed using XPREP (as part of the APEX v2.2.0 software), and solved by either direct (SHELXS-97)[80] or intrinsic (SHELXT)[81] methods. The structures were completed by difference Fourier synthesis and refined with full-matrix least-squares procedures based on F^2. In all cases, non-hydrogen atoms were refined anisotropically and hydrogen atoms were generated in ideal positions and then updated with each cycle of refinement {with the exception of hydrogen atoms on Mn or Si (except ***trans*H_2-4b** where this only applies to the terminal metal hydride) which were located from the difference map and refined isotropically}. Refinement was carried out using Olex2.[82]

Complexes **1a-b**, **2a-b**, **3a-b**, and **4a-b** are air sensitive, and products observed upon reaction with air are malodorous. Therefore, all syntheses were conducted under an atmosphere of argon.

[(dmpe)$_2$MnH$_2$(SiH$_2$Ph)] (4a). 209.5 mg (0.367 mmol) of [(dmpe)$_2$MnH(SiH$_2$Ph)$_2$] (**2a**) was dissolved in 10 mL of benzene. The reaction mixture was freeze/pump/thawed in a 50 mL storage flask three times, and then was placed under 1 atm of H_2 at –95 °C, sealed, and warmed to room temperature. After stirring at room temperature for 2 days, the solvent was removed *in vacuo*. The resulting yellow solid was recrystallized from a concentrated solution of hexanes at –30 °C giving a yellow powder which was dried *in vacuo*; 111.1 mg. Concentrating the mother liquor and leaving it at –30 °C yielded an additional 20.9 mg of **4a**, for a total yield of 132.0 mg (0.284 mmol, 77 %). X-ray quality crystals were obtained from hexanes. ^{1}H NMR (d^8-toluene, 600 MHz, 298 K): δ 8.00 (br. s, 2H, *o*-ph), 7.29 (t, 2H, $^3J_{H,H}$ 7.4 Hz, *m*-ph), 7.18 (t, 1H, $^3J_{H,H}$ 7.1 Hz, *p*-ph), 5.45 (br. s, 2H, Si*H*), 1.5–0.9 (br. singlets, 32H, PC*H*$_3$ and PC*H*$_2$), –12.54 (br. s, 1H, Mn*H*). ^{13}C{^{1}H} NMR (d^8-toluene, 151 MHz, 298 K): δ 135.83 (s, *o*-ph), 127.28 (s, *m*-ph), 126.82 (s, *p*-ph), 33.13 (br. s,). ^{31}P{^{1}H} NMR (d^8-toluene, 202 MHz, 298 K): δ 76.69 (br. s). ***central*-4a**: ^{1}H NMR (d^8-toluene, 500 MHz, 186 K): δ 8.37 (d, 2H, $^3J_{H,H}$ 7.2 Hz, *o*-ph), 7.49 (t, 2H, $^3J_{H,H}$ 7.2 Hz, *m*-ph), 7.34 (t, 1H, $^3J_{H,H}$ 7.0 Hz, *p*-ph), 6.10 (s with ^{29}Si sat., 1H, $^1J_{Si,H}$ 171.4 Hz, Si*H*), 6.02 (t with ^{29}Si sat., 1H, $^3J_{H,P}$ 9.5 Hz, $^1J_{Si,H}$ 175.6 Hz, Si*H*), 0.8-1.5 (various m, 8H, PC*H*$_2$), 1.39 (d, 6H, $^2J_{H,P}$ 2.9 Hz, PC*H*$_3$), 1.30 (s, 6H, PC*H*$_3$), 0.96 (s, 6H, PC*H*$_3$), 0.74 (s, 6H, PC*H*$_3$), –12.83 (m, 2H, Mn*H*). ^{13}C{^{1}H} NMR (C$_6$D$_6$, 126 MHz, 207 K): δ 151.39 (s, *i*-ph), 135.59 (s, *o*-ph), 127.30 (s, *m*-ph), 127.04 (s, *p*-ph), 33.44 (m, P*C*H$_2$), 32.35 (m, P*C*H$_2$), 30.13 (t, $J_{C,P}$ 15 Hz, P*C*H$_3$), 22.56 (s, P*C*H$_3$), 22.30 (d, $^2J_{C,P}$ 16 Hz, P*C*H$_3$), 21.57 (m, P*C*H$_3$). ^{29}Si{^{1}H} NMR (d^8-toluene, 119 MHz, 226 K): δ –15.73 (s). ^{31}P{^{1}H} NMR (d^8-toluene, 202 MHz, 186 K): δ 73.98 (br. s, 2P), 72.38 (br. s, 2P). ***transHSi*-4a**: ^{1}H NMR (d^8-toluene, 500 MHz, 186 K): δ 8.15 (d, 2H, $^3J_{H,H}$ 7.1 Hz, *o*-ph), 7.40 (t, 2H, $^3J_{H,H}$ 7.1 Hz, *m*-ph), 7.25 (t, 1H, $^3J_{H,H}$ 7.1 Hz, *p*-ph), 5.46 (s with ^{29}Si sat., 2H, $^1J_{Si,H}$ 155.0 Hz, Si*H*), 0.8-1.5 (various m, 8H, PC*H*$_2$), 1.34 (s, 12H, PC*H*$_3$), 1.07 (s, 12H, PC*H*$_3$), –10.88 (p, 1H, $^2J_{H,P}$ 53.9 Hz, Mn*H*), –12.66 (p, 1H, $^2J_{H,P}$ 23.1 Hz, Mn*H*Si). ^{13}C{^{1}H} NMR (C$_6$D$_6$, 126 MHz, 207 K): δ 149.71 (s, *i*-ph), 135.95 (s, *o*-ph), 127.30 (s, *m*-ph), 126.80 (s, *p*-ph), 32.25 (m, P*C*H$_2$), 27.73 (m, P*C*H$_3$), 20.8 (P*C*H$_3$)[83]. ^{29}Si{^{1}H} NMR (d^8-toluene, 119 MHz, 226 K): δ –1.63 (m). ^{31}P{^{1}H} NMR (d^8-toluene, 202 MHz, 186 K): δ 77.85 (s). *ν*(SiH, MnH) (Nujol, cm^{-1}): 1808, 1973, 2025, 2056. *ν*(SiH, MnH) (hexanes, cm^{-1}): 1738, 1756, 1811, 1990, 2014. Anal. Found (calcd.): C, 46.72 (46.55); H, 8.85 (8.90).

[(dmpe)$_2$MnH$_2$(SiH$_2$^{n}Bu)] (4b). 108.9 mg (0.205 mmol) of [(dmpe)$_2$MnH(SiH$_2$^{n}Bu)$_2$] (**2b**) was dissolved in 10 mL of benzene. The reaction mixture was freeze/pump/thawed in a 50 mL storage flask three times, and then was placed under 1 atm of H_2 at –95 °C, sealed, and warmed to room temperature. After stirring at room temperature for 3 days, the solvent was removed *in vacuo*. The resulting yellow solid was recrystallized from a concentrated solution of hexanes at –30 °C and dried *in vacuo* to afford a yellow powder. Yield = 41.6 mg (0.094 mmol, 46 %). X-ray quality crystals were obtained from a dilute solution in hexanes at –30 °C. ^{1}H NMR (d^8 toluene, 600 MHz, 298 K): δ 4.65 (br. s, 2H, Si*H*), 1.76 (p, 2H, $^3J_{H,H}$ 7.6 Hz, SiH$_2$CH$_2$C*H*$_2$CH$_2$CH$_3$), 1.58 (s, 2H, $^3J_{H,H}$ 7.4 Hz, SiH$_2$CH$_2$CH$_2$C*H*$_2$CH$_3$), 1.34 (br. s, 8H, PC*H*$_2$), 1.23 (br. s, 24H, PC*H*$_3$), 1.04 (t, 3H, $^3J_{H,H}$ 7.3 Hz, SiH$_2$CH$_2$CH$_2$CH$_2$C*H*$_3$), 0.89 (br. s, 2H, SiH$_2$C*H*$_2$CH$_2$CH$_2$CH$_3$), –12.54 (br. s, 2H, Mn*H*). ^{13}C{^{1}H} NMR (d^8 toluene, 151 MHz, 298 K): δ 33.24 (br. s, P*C*H$_2$), 32.86 (s, SiH$_2$CH$_2$*C*H$_2$CH$_2$CH$_3$), 27.07 (s, SiH$_2$CH$_2$CH$_2$*C*H$_2$CH$_3$), 14.60 (s, SiH$_2$CH$_2$CH$_2$CH$_2$*C*H$_3$). ^{31}P NMR (d^8 toluene, 243 MHz, 298 K): δ 76.51 (s). ***central*-4b**: ^{1}H NMR (d^8 toluene, 500 MHz, 207 K): δ 5.39 (s with ^{29}Si sat., 1H, $^1J_{Si,H}$ 160.4 Hz, Si*H*), 5.24 (s with ^{29}Si sat., 1H, $^1J_{Si,H}$ 168.4 Hz, Si*H*), 2.01 (m, 2H, SiH$_2$CH$_2$C*H*$_2$CH$_2$CH$_3$), 1.77 (m, 2H, SiH$_2$CH$_2$CH$_2$C*H*$_2$CH$_3$), 1.41 (s, 6H, PC*H*$_3$), 1.40 (m, 2H, PC*H*$_2$),1.36 (m, 1H, SiH$_2$C*H*$_2$CH$_2$CH$_2$CH$_3$), 1.26 (s, 6H, PC*H*$_3$), 1.21 (m, 2H, PC*H*$_2$), 1.18 (s, 6H, PC*H*$_3$), 1.18 (m, 1H, SiH$_2$C*H*$_2$CH$_2$CH$_2$CH$_3$), 1.18 (t, 3H, $^3J_{H,H}$ 7.4 Hz,[84] SiH$_2$CH$_2$CH$_2$CH$_2$C*H*$_3$), 0.99 (m, 2H, PC*H*$_2$), 0.88 (m, 2H, PC*H*$_2$), 0.79 (s, 6H, PC*H*$_3$), –12.75 (m, 2H, Mn*H*). ^{13}C{^{1}H} NMR (d^8 toluene, 126 MHz, 207 K): δ 33.46 (m, P*C*H$_2$), 32.37 (m, P*C*H$_2$), 32.37 (s, SiH$_2$CH$_2$*C*H$_2$CH$_2$CH$_3$), 30.48 (m, P*C*H$_3$), 27.49 (s, SiH$_2$*C*H$_2$CH$_2$CH$_2$CH$_3$), 27.49 (s, SiH$_2$CH$_2$CH$_2$*C*H$_2$CH$_3$), 22.64 (s, P*C*H$_3$), 22.25 (m, P*C*H$_3$), 15.04 (s, SiH$_2$CH$_2$CH$_2$CH$_2$*C*H$_3$). ^{29}Si{^{1}H} NMR (d^8 toluene, 119 MHz, 207 K): δ –22.00. ^{31}P{^{1}H} NMR (d^8 toluene, 243 MHz, 205 K): δ 74.06 (br. s, 2P), 72.05 (br. s, 2P). ***transHSi*-4b**: (d^8 toluene, 500 MHz, 207 K): δ 4.72 (s with ^{29}Si sat., 2H, $^1J_{Si,H}$ 151.7 Hz, Si*H*), 1.92 (m, 2H, SiH$_2$CH$_2$C*H*$_2$CH$_2$CH$_3$), 1.69 (m, 2H, $^3J_{H,H}$ 7.3 Hz, SiH$_2$CH$_2$CH$_2$C*H*$_2$CH$_3$), 1.56 (br. s, 4H, PC*H*$_2$), 1.36 (s, 12H, PC*H*$_3$), 1.26 (br. s, 4H, PC*H*$_2$), 1.12 (s, 12H, PC*H*$_3$), 1.12 (t, 3H, $^3J_{H,H}$ 7.3 Hz,[84] SiH$_2$CH$_2$CH$_2$CH$_2$C*H*$_3$), 0.99 (m, 2H, SiH$_2$C*H*$_2$CH$_2$CH$_2$CH$_3$), –11.25 (p, 1H, $^2J_{H,P}$ 51.5 Hz, Mn*H*), –13.28 (p, 1H, ^{2}J$_{H,P}$ 23.0 Hz, Mn*H*Si). ^{13}C{^{1}H} NMR (d^8 toluene, 126 MHz, 207 K): δ 33.46 (s, SiH$_2$CH$_2$*C*H$_2$CH$_2$CH$_3$), 32.37 (m, P*C*H$_2$), 27.62 (s, SiH$_2$CH$_2$CH$_2$*C*H$_2$CH$_3$), 27.49 (s, P*C*H$_3$), 22.82 (s, SiH$_2$*C*H$_2$CH$_2$CH$_2$CH$_3$), 20.78 (s, P*C*H$_3$), 14.91 (s, SiH$_2$CH$_2$CH$_2$CH$_2$*C*H$_3$). ^{29}Si{^{1}H} NMR (d^8 toluene, 119 MHz, 207 K): –6.91. ^{31}P{^{1}H} NMR (d^8 toluene, 243 MHz, 205 K): 77.48 (s). *ν*(SiH, MnH) (Nujol, cm^{-1}): 1740, 1965, 1995. *ν*(SiH, MnH) (hexanes, cm^{-1}): 1737, 1830, 1983, 2013. Anal. Found (calcd.): C, 43.39 (43.24); H, 9.94 (10.20).

[(dmpe)$_2$MnD$_2$(SiH$_2$R)] (4a_d$_2$: R = Ph, 4b_d$_2$: R = ^{n}Bu). Roughly 10 mg of the manganese-containing precursor used to synthesize the fully protonated complexes {for **4a** [(dmpe)$_2$MnH(SiH$_2$Ph)$_2$] (**2a**) and for **4b** [(dmpe)$_2$MnH(SiH$_2$^{n}Bu)$_2$] (**2b**)} was dissolved in roughly 1 mL of C$_6$D$_6$. The reaction mixture was freeze/pump/thawed in a J-young NMR tube three times, and then was placed under 1 atm of D_2 at –95 °C, sealed, and warmed to room temperature and then allowed to sit at room temperature for the reaction times required to prepare the protio analogues. The deuterated complexes were isolated from free hydrosilane by-prodcts on the NMR scale by removing the solvent and hydrosilane *in vacuo*, and used without further purification. NMR spectra of **4a_d$_2$** and **4b_d$_2$** differ from the protonated analogues by the absence of peaks in the ^{1}H NMR spectra corresponding to the Mn*H* environments.

IR data for 3a. *ν*(SiH, MnH) (Nujol, cm^{-1}): 1767, 1807, 1974.

IR data for 3b. *ν*(SiH, MnH) (Nujol, cm^{-1}): 1877 (with shoulder to lower wavenumber), 2015. *ν*(SiH, MnH) (hexanes, cm^{-1}): 1734, 1864, 2031 (with two shoulders to lower wavenumber).

ASSOCIATED CONTENT

Supporting Information

^{29}Si_edited ^{1}H–^{1}H COSY NMR spectra for **2a-b**, **3a-b**, and **4a-b**, ^{1}H–^{1}H{^{31}P} dqf COSY NMR spectra for **3a-b** and **4b**, ^{1}H–^{1}H dqf COSY NMR spectra for **3b** and **4b**, table of ^{1}H–^{1}H COSY NMR parameters used for experiments when measuring $J_{Si,H}$, symbolic pulse sequences for ^{1}H–^{1}H{^{31}P} dqf COSY and ^{29}Si_edited ^{1}H–^{1}H COSY NMR experiments, computational results (tables of energies

and Hirschfeld charges for all complexes, tables of bonding parameters and bond orders for PH_3 analogues), visualization of calculated structures, tables of crystal data/crystal structure refinement, selected 1D NMR spectra for complexes **4a-b**, **4a _d**$_2$, and **4b_d**$_2$, and IR spectra for complexes **3a-b** and **4a-b** (PDF)

Cartesian coordinates of the calculated structures (XYZ)

Accession Codes

CCDC 1896287 and 1896288 contain the supplementary crystallographic data for complexes **4a** and **4b**. These data can be obtained free of charge via www.ccdc.cam.ac.uk/data_request/cif, or by emailing data_request@ccdc.cam.ac.uk, or by contacting The Cambridge Crystallographic Data Centre, 12 Union Road, Cambridge CB2 1EZ, UK; fax: +44 1223 336033.

AUTHOR INFORMATION

Corresponding Author

* D.J.H.E.: tel, 905-525-9140 x23307; fax, 905-522-2509; e-mail, emslied@mcmaster.ca.

Notes

The authors declare no competing financial interest.

ACKNOWLEDGMENT

D.J.H.E. thanks the NSERC of Canada for a Discovery Grant. We are grateful to Dr. Jim Britten of the McMaster Analytical X-ray Diffraction Facility and Dr. Ignacio Vargas-Baca of McMaster University Department of Chemistry for advice and support with X-ray diffraction and DFT calculations respectively. Also, we are grateful to Compute Canada for access to computational resources.

REFERENCES

1. Schubert, U. η^2 Coordination of Si–H σ Bonds to Transition Metals, *Adv. Organomet. Chem.* **1990**, *30*, 151-187.

2. For general reviews of this field, see (a) Crabtree, R. H. Transition Metal Complexation of σ Bonds, *Angew. Chem. Int. Ed. Engl.* **1993**, *32*, 789-805. (b) Corey, J. Y.; Braddock-Wilking, J. Reactions of Hydrosilanes with Transition-Metal Complexes: Formation of Stable Transition-Metal Silyl Compounds, *Chem. Rev.* **1999**, *99*, 175-292. (c) Lin, Z. Structural and bonding characteristics in transition metal–silane complexes, *Chem. Soc. Rev.* **2002**, *31*, 239-245. (d) Corey, J. Y. Reactions of Hydrosilanes with Transition Metal Complexes and Characterization of the Products, *Chem. Rev.* **2011**, *111*, 863-1071. (e) Corey, J. Y. Reactions of Hydrosilanes with Transition Metal Complexes, *Chem. Rev.* **2016**, *116*, 11291-11435.

3. Selected early contributions to this field include (a) Schubert, U.; Ackermann, K.; Wörle, B. A Long Si–H Bond or a Short Si–H Nonbond? Neutron Diffraction Study of $(\eta^5\text{-}CH_3C_5H_4)(CO)_2(H)MnSiF(C_6H_5)_2$, *J. Am. Chem. Soc.* **1982**, *104*, 7378-7380. (b) Rabaâ, H.; Saillard, J. Y.; Schubert, U. Interaction between a σ bond and a d^n ML_n fragment: an MO analysis of the MnSiH three-center interaction in $CpMnL_2HSiR_3$ complexes, *J. Organomet. Chem.* **1987**, *330*, 397-413. (c) Schubert, U.; Schwarz, M.; Möller, F. Silicon-Containing Carbene Complexes. 15. A Strong W···H···Si Interaction in the 16-Electron Carbene Complex $(CO)_4WC(NMe_2)SiHMes_2$, *Organometallics* **1994**, *13*, 1554-1555. (d) Schubert, U.; Gilges, H. Transition Metal Silyl Complexes. 53. Magnitude of the Chelate Effect in the Oxidative Addition of Si–H Bonds, *Organometallics* **1996**, *15*, 2373-2375.

4. Hoyano, J.; Elder, M.; Graham, W. A. G. Hydrogen-Bridged Silicon-Rhenium Bonds. A Diphenylsilane Complex of Rhenium Carbonyl, *J. Am. Chem. Soc.* **1969**, *91*, 4568-4569.

5. Kubas, G. J.; Ryan, R. R.; Swanson, B. I.; Vergamini, P. J.; Wasserman, H. J. Characterization of the First Examples of Isolable Molecular Hydrogen Complexes, $M(CO)_3(PR_3)_2(H_2)$ (M = Mo, W; R = Cy, *i*-Pr). Evidence for a Side-on Bonded H_2 Ligand, *J. Am. Chem. Soc.* **1984**, *106*, 451-452.

6. Graham, W. A. G.; Hart-Davis, A. J. Silicon-Transition Metal Chemistry. VI. Kinetics and Mechanism of the Replacement of Triphenylsilane by Triphenylphosphine in Hydridotriphenylsilyl (π-cyclopentadienyl)dicarbonylmanganese, *J. Am. Chem. Soc.* **1971**, *93*, 4388-4393.

7. Nikonov, G. I. New types of non-classical interligand interactions involving silicon based ligands, *J. Organomet. Chem.* **2001**, *635*, 24-36.

8. Nikonov, G. I. Recent Advances in Nonclassical Interligand Si··· H Interactions, *Adv. Organomet. Chem.* **2005**, *53*, 217-309.

9. Lachaize, S.; Sabo-Etienne, S. σ-Silane Ruthenium Complexes: The Crucial Role of Secondary Interactions, *Eur. J. Inorg. Chem.* **2006**, 2115-2127.

10. A variety of terms have been used to describe Si–H interactions in nonclassical hydrosilane complexes including stretched σ-bonding or Si-H bonding (ref. 2a), α-agostic interactions (Spencer, M. D.; Shelby, Q. D.; Girolami, G. S. Titanium-Catalyzed Dehydrocoupling of Silanes: Direct Conversion of Primary Monosilanes to Titanium(0) Oligosilane Complexes with Agostic α-Si–H···Ti Interactions, *J. Am. Chem. Soc.* **2007**, *129*, 1860-1861), Interligand Hypervalent Interactions (IHI; refs. 12a, 13), and Secondary Interactions between Silicon and Hydrogen Atoms (SISHA; ref. 9).

11. Complexes featuring interligand Si–H interactions are sometimes refered to as hybrids between σ-hydrosilane and silyl hydride complexes (ref. 78), or complexes featuring incomplete (or arrested) oxidative addition some. The latter are sometimes divided further into asymmetric oxidative addition products (ASOAPs), typically featuring significant Si–H interactions and negative $J_{Si,H}$ coupling constants, and symmetric oxidative addition products (SOAPs), featuring very weak residual Si–H interactions and positive $J_{Si,H}$ coupling constants (refs 26a,c and 28).

12. (a) Nikonov, G. I.; Kuzmina, L. G.; Lemenovskii, D. A.; Kotov, V. V. Interligand Hypervalent Interaction in the Bis(silyl) Hydride Derivatives of Niobocene, *J. Am. Chem. Soc.* **1995**, *117*, 10133-10134. (b) Nikonov, G. I.; Mountford, P.; Ignatov, S. K.; Green, J. C.; Leech, M. A.; Kuzmina, L. G.; Razuvaev, A. G.; Rees, N. H.; Blake, A. J.; Howard, J. A. K.; Lemenovskii, D. A. Surprising diversity of non-classical silicon-hydrogen interactions in half-sandwich complexes of Nb and Ta: M–H···Si–Cl interligand hypervalent interaction (IHI) *versus* stretched and unstretched β-Si–H···M agostic bonding, *J. Chem. Soc., Dalton Trans.* **2001**, 2903-2915. (c) Dubberley, S. R.; Ignatov, S. K.; Rees, N. H.; Razuvaev, A. G.; Mountford, P.; Nikonov, G. I. Are *J*(Si–H) NMR Coupling Constants Really a Probe for the Existence of Nonclassical H–Si Interactions?, *J. Am. Chem. Soc.* **2003**, *125*, 642-643. (d) Nikonov, G. I.; Mountford, P.; Dubberley, S. R. Tantalizing Chemistry of the Half-Sandwich Silylhydride Complexes of Niobium: Identification of Likely Intermediates on the Way to Agostic Complexes, *Inorg. Chem.* **2003**, *42*, 258-260. (e) Dorogov, K. Y.; Yousufuddin, M.; Ho, N.-N.; Churakov, A. V.; Kuzmina, L. G.; Schultz, A. J.; Mason, S. A.; Howard, J. A. K.; Lemenovskii, D. A.; Bau, R.; Nikonov, G. I. Syntheses and Structures of Asymmetric Bis(silyl) Niobocene Hydrides, *Inorg. Chem.* **2007**, *46*, 147-160. (f) Gutsulyak, D. V.; Churakov, A. V.; Kuzmina, L. G.; Howard, J. A. K.; Nikonov, G. I. Steric and Electronic Effects in Half-Sandwich Ruthenium Silane *σ*-Complexes with Si–H and Si–Cl Interligand Interactions, *Organometallics* **2009**, *28*, 2655-2657. (g) Gutsulyak, D. V.; Vyboishchikov, S. F.; Nikonov, G. I. Cationic Silane *σ*-complexes of Ruthenium with Relevance to Catalysis, *J. Am. Chem. Soc.* **2010**, *132*, 5950-5951. (h) Khalimon, A. Y.; Ignatov, S. K.; Okhapkin, A. I.; Simionescu, R.; Kuzmina, L. G.; Howard, J. A. K.; Nikonov, G. I. Unusual Structure, Fluxionality, and Reaction Mechanism of Carbonyl Hydrosilylation by Silyl Hydride Complex $[(ArN=)Mo(H)(SiH_2Ph)(PMe_3)_3]$, *Chem. - Eur. J.* **2013**, *19*, 8573-8590. (i) Khalimon, A. Y.; McLeod, N. A.; Ignatov, S. K.; Okhapkin, A. I.; Kuzmina, L. G.; Howard, J. A. K.; Nikonov, G. I. Multiple coupling of silanes with imido complexes of Mo, *Dalton Trans.* **2014**, *43*, 8446-8453. (j) Mai, V. H.; Korobkov, I.; Nikonov, G. I. Half-

Sandwich Silane σ-Complexes of Ruthenium Supported by NHC Carbene, *Organometallics* **2016**, *35*, 936-942.

13. Nikonov, G. I.; Kuzmina, L. G.; Vyboishchikov, S. F.; Lemenovskii, D. A.; Howard, J. A. K. Niobocene Silyl Hydride Complexes with Nonclassical Interligand Hypervalent Interactions, *Chem. - Eur. J.* **1999**, *5*, 2947-2964.

14. Duckett, S. B.; Kuzmina, L. G.; Nikonov, G. I. Fine tuning of Si–H interligand hypervalent interactions (IHI) in half-sandwich silyl hydrido complexes of ruthenium, *Inorg. Chem. Commun.* **2000**, *3*, 126-128.

15. Osipov, A. L.; Gerdov, S. M.; Kuzmina, L. G.; Howard, J. A. K.; Nikonov, G. I. Syntheses and X-ray Diffraction Studies of Half-Sandwich Hydridosilyl Complexes of Ruthenium, *Organometallics* **2005**, *24*, 587-602.

16. Vybioshchikov, S. F.; Nikonov, G. I. Unique {$H(SiR_3)_2$}, (H_2SiR_3), $H(HSiR_3)$, and (H_2)SiR_3 Ligand Sets Supported by the {Fe(Cp)(L)} Platform (L = CO, PR_3), *Chem. - Eur. J.* **2006**, *12*, 8518-8533.

17. Vyboishchikov, S. F.; Nikonov, G. I. Rhodium Silyl Hydrides in Oxidation State +5: Classical or Nonclassical?, *Organometallics* **2007**, *26*, 4160-4169.

18. Gutsulyak, D. V.; Kuzmina, L. G.; Howard, J. A. K.; Vyboishchikov, S. F.; Nikonov, G. I. $Cp(Pr^i_2MeP)FeH_2SiR_3$: Nonclassical Iron Silyl Dihydride, *J. Am. Chem. Soc.* **2008**, *130*, 3732-3733.

19. Mai, V. H.; Kuzmina, L. G.; Churakov, A. V.; Korobkov, I.; Howard, J. A. K.; Nikonov, G. I. NHC carbene supported half-sandwich hydridosilyl complexes of ruthenium: the impact of supporting ligands on Si···H interligand interactions, *Dalton Trans.* **2016**, *45*, 208-215.

20. Delpech, F.; Sabo-Etienne, S.; Donnadieu, B.; Chaudret, B. Stoichiometric and Catalytic Activation of Allyldimethylsilane. Synthesis of $[RuH_2\{\eta^4\text{-}HSiMe_2(CH{=}CHMe)\}(PCy_3)_2]$, *Organometallics* **1998**, *17*, 4926-4928.

21. Atheaux, I.; Delpech, F.; Donnadieu, B.; Sabo-Etienne, S.; Chaudret, B.; Hussein, K.; Barthelat, J.-C.; Braun, T.; Duckett, S. B.; Perutz, R. N. Exchange Processes in Complexes with Two Ruthenium (η^2-Silane) Linkages: Role of the Secondary Interactions between Silicon and Hydrogen Atoms, *Organometallics* **2002**, *21*, 5347-5357.

22. Lachaize, S.; Sabo-Etienne, S.; Donnadieu, B.; Chaudret, B. Mechanistic studies on ethylene silylation with chlorosilanes catalyzed by ruthenium complexes, *Chem. Commun. (Cambridge, U. K.)* **2003**, 214-215.

23. (a) Montiel-Palma, V.; Piechaczyk, O.; Picot, A.; Auffrant, A.; Vendier, L.; Le Floch, P.; Sabo-Etienne, S. Bonding Mode of a Bifunctional P~Si–H Ligand in the Ruthenium Complex "$Ru(PPh_2CH_2OSiMe_2H)_3$", *Inorg. Chem.* **2008**, *47*, 8601-8603. (b) Montiel-Palma, V.; Muñoz-Hernández, M. A.; Cuevas-Chávez, C. A.; Vendier, L.; Grellier, M.; Sabo-Etienne, S. Phosphinodi(benzylsilane) $PhP\{(o\text{-}C_6H_4CH_2)SiMe_2H\}_2$: A Versatile "$PSi_2H_x$" Pincer-Type Ligand at Ruthenium, *Inorg. Chem.* **2013**, *52*, 9798-9806.

24. Grellier, M.; Ayed, T.; Barthelat, J.-C.; Albinati, A.; Mason, S.; Vendier, L.; Coppel, Y.; Sabo-Etienne, S. Versatile Coordination of 2-Pyridinetetramethyldisilazane at Ruthenium: Ru(II) vs Ru(IV) As Evidenced by NMR, X-ray, Neutron, and DFT Studies, *J. Am. Chem. Soc.* **2009**, *131*, 7633-7640.

25. (a) Smart, K. A.; Grellier, M.; Vendier, L.; Mason, S. A.; Capelli, S. C.; Albinati, A.; Sabo-Etienne, S. Step-by-Step Introduction of Silazane Moieties at Ruthenium: Different Extents of Ru–H–Si Bond Activation, *Inorg. Chem.* **2013**, *52*, 2654-2661. (b) Smart, K. A.; Grellier, M.; Coppel, Y.; Vendier, L.; Mason, S. A.; Capelli, S. C.; Albinati, A.; Montiel-Palma, V.; Muñoz-Hernández, M. A.; Sabo-Etienne, S. Nature of Si–H Interactions in a Series of Ruthenium Silazane Complexes Using Multinuclear Solid-State NMR and Neutron Diffraction, *Inorg Chem* **2014**, *53*, 1156-1165.

26. (a) Scherer, W.; Eickerling, G.; Tafipolsky, M.; McGrady, G. S.; Sirsch, P.; Chatterton, N. P. Elucidation of the bonding in Mn(η^2-SiH) complexes by charge density analysis and T_1 NMR measurements: asymmetric oxidative addition and anomeric effects at silicon, *Chem. Commun. (Cambridge, U. K.)* **2006**, 2986-2988. (b) Scherer, W.; Meixner, P.; Barquera-Lozada, J. E.; Hauf, C.; Obenhuber, A.; Brück, A.; Wolstenholme, D. J.; Ruhland, K.; Leusser, D.; Stalke, D. A Unifying Bonding Concept for Metal Hydrosilane Complexes, *Angew. Chem., Int. Ed.* **2013**, *52*, 6092-6096. (c) Hauf, C.; Barquera-Lozada, J. E.; Meixner, P.; Eickerling, G.; Altmannshofer, S.; Stalke, D.; Zell, T.; Schmidt, D.; Radius, U.; Scherer, W. Remanent Si–H Interactions in Late Transition Metal Silane Complexes, *Z. Anorg. Allg. Chem.* **2013**, *639*, 1996-2004.

27. Scherer, W.; Meixner, P.; Batke, K.; Barquera-Lozada, J. E.; Ruhland, K.; Fischer, A.; Eickerling, G.; Eichele, K. *J*(Si,H) Coupling Constants in Nonclassical Transition-Metal Silane Complexes, *Angew. Chem., Int. Ed.* **2016**, *55*, 11673-11677.

28. Meixner, P.; Batke, K.; Fischer, A.; Schmitz, D.; Eickerling, G.; Kalter, M.; Ruhland, K.; Eichele, K.; Barquera-Lozada, J. E.; Casati, N. P. M.; Montisci, F.; Macchi, P.; Scherer, W. *J*(Si,H) Coupling Constants of Activated Si–H Bonds, *J. Phys. Chem. A* **2017**, *121*, 7219-7235.

29. Examples include (a) Fan, M.-F.; Jia, G.; Lin, Z. Metal–Silane Interaction in the Novel Pseudooctahedral Silane Complex *cis*-$Mo(CO)(PH_3)_4(H\cdots SiH_3)$ and Some Related Isomers: An *ab Initio* Study, *J. Am. Chem. Soc.* **1996**, *118*, 9915-9921. (b) Fan, M.-F.; Lin, Z. Peculiar Hydride–Silyl Interactions in Group 5 Bent Metallocene Complexes, Studied by ab Initio Calculations, *Organometallics* **1998**, *17*, 1092-1100. (c) Lichtenberger, D. L. Electron Distribution, Bonding, and *J*(Si–H) NMR Coupling Constant in (η^5-C_5H_5)$(CO)_2MnHSiCl_3$: The Molecular Orbital View, *Organometallics* **2003**, *22*, 1599-1602. (d) Bader, R. F. W.; Matta, C. F.; Cortés-Guzmán, F. Where To Draw the Line in Defining a Molecular Structure, *Organometallics* **2004**, *23*, 6253-6263. (e) McGrady, G. S.; Sirsch, P.; Chatterton, N. P.; Ostermann, A.; Gatti, C.; Altmannshofer, S.; Herz, V.; Eickerling, G.; Scherer, W. Nature of the Bonding in Metal-Silane σ-Complexes, *Inorg. Chem.* **2009**, *48*, 1588-1598.

30. Ignatov, S. K.; Rees, N. H.; Tyrrell, B. R.; Dubberley, S. R.; Razuvaev, A. G.; Mountford, P.; Nikonov, G. I. Nonclassical Titanocene Silyl Hydrides, *Chem. - Eur. J.* **2004**, *10*, 4991-4999.

31. Alcaraz, G.; Sabo-Etienne, S. NMR: A good tool to ascertain σ-silane or σ-borane formulations?, *Coord. Chem. Rev.* **2008**, *252*, 2395-2409.

32. For pioneering early work using $J_{Si,H}$ to analyze interligand Si–H interactions from magnitude alone see; Colomer, E.; Corriu, R. J. P.; Marzin, C.; Vioux, A. Study of the Insertion Products of Manganese in the Silicon-Hydrogen Bond. Nature of the Bond and Proton Exchange in the H–Mn–Si–H system, *Inorg. Chem.* **1982**, *21*, 368-373.

33. Berger, S.; Braun, S., *200 and More NMR Experiments: A Practical Course*. Wiley-VCH: Weinheim, 2004.

34. (a) Schraml, J.; Bellama, J., ^{29}Si Nuclear Magnetic Resonance. In *Determination of Organic Structures by Phyical Methods*, Nachod, F.; Zuckerman, J.; Randall, E., Eds. Academic Press: New York, 1976; Vol. 6, pp 203-270. (b) Harris, R. K.; Kennedy, J. D.; McFarlane, W., Group IV-Silicon, Germanium, Tin and Lead. In *NMR and the Periodic Table*, Harris, R. K.; Mann, B. E., Eds. Academic Press: New York, USA, 1978; pp 309-377.

35. For a review of complexes with multiple nonclassical Si–H interactions invovling a single Si atom, see Nikonov, G. I. Going Beyond σ Complexation: Nonclassical Interligand Interactions of Silyl Groups with Two and More Hydrides, *Angew. Chem., Int. Ed.* **2001**, *40*, 3353-3355.

36. For examples of computational reports on complexes with multiple nonclassical Si–H interactions involving a single Si, see (a). Lin, Z.; Hall, M. B. Hydride Locations and Bonding Studies in Some Silyl Polyhydride Rhenium Complexes, *Inorg. Chem.* **1991**, *30*, 2569-2572. (b) Ray, M.; Nakao, Y.; Sato, H.; Sakaki, S.; Watanabe, T.; Hashimoto, H.; Tobita, H. Experimental and Theoretical Study of a Tungsten Dihydride Silyl Complex: New Insight into Its Bonding Nature and Fluxional Behavior, *Organometallics* **2010**, *29*, 6267-6281.

37. Luo, X. L.; Crabtree, R. H. Homogeneous Catalysis of Silane Alcoholysis via Nucleophilic Attack by the Alcohol on an Ir(η^2-$HSiR_3$) intermediate catalyzed by $[IrH_2S_2(PPh_3)_2]SbF_6$ (S = Solvent), *J. Am. Chem. Soc.* **1989**, *111*, 2527-2535.

38. (a) Luo, X. L.; Baudry, D.; Boydell, P.; Charpin, P.; Nierlich, M.; Ephritikhine, M.; Crabtree, R. H. Reaction of $ReH_7(PPh_3)_2$ with Silanes: Preparation and Characterization of the First

Silyl Polyhydride Complexes, $ReH_6(SiR_3)(PPh_3)_2$ (SiR_3 = $SiPh_3$, $SiEt_3$, $SiHEt_2$), *Inorg. Chem.* **1990**, *29*, 1511-1517. (b) Luo, X. L.; Schulte, G. K.; Demou, P.; Crabtree, R. H. Unusual Stereochemical Rigidity in Seven-Coordination. Synthesis and Structural Characterization of $ReH_2(EPh_3)(CO)(PMe_2Ph)_3$ (E = Si, Sn), *Inorg. Chem.* **1990**, *29*, 4268-4273.

39. Jagirdar, B. R.; Palmer, R.; Klabunde, K. J.; Radonovich, L. J. Metal Hydride vs Side-on σ-Bonded Trichlorosilane Complexes of Arene–Chromium Derivatives: (η^6-arene)Cr(CO)$(H)_2(SiCl_3)_2$, *Inorg. Chem.* **1995**, *34*, 278-283.

40. Hussein, K.; Marsden, C. J.; Barthelat, J.-C.; Rodriguez, V.; Conejero, S.; Sabo-Etienne, S.; Donnadieu, B.; Chaudret, B. X-Ray structure and theoretical studies of $RuH_2(\eta^2\text{-}H_2)(\eta^2\text{-H-}SiPh_3)(PCy_3)_2$, a complex with two different η^2-coordinated σ bonds, *Chem. Commun. (Cambridge)* **1999**, 1315-1316.

41. Mautz, J.; Heinze, K.; Wadepohl, H.; Huttner, G. Reductive Activation of *tripod* Metal Compounds: Identification of Intermediates and Preparative Application, *Eur. J. Inorg. Chem.* **2008**, 1413-1422.

42. Lee, T. Y.; Dang, L.; Zhou, Z.; Yeung, C. H.; Lin, Z.; Lau, C. P. Nonclassical Ruthenium Silyl Dihydride Complexes $TpRu(PPh_3)(\eta^3\text{-}HSiR_3H)$ [Tp = Hydridotris(pyrazolyl)borate]: Catalytic Hydrolytic Oxidation of Organosilanes to Silanols with $TpRu(PPh_3)(\eta^3\text{-}HSiR_3H)$, *Eur. J. Inorg. Chem.* **2010**, 5675-5684.

43. Fasulo, M. E.; Calimano, E.; Buchanan, J. M.; Tilley, T. D. Multiple Si–H Bond Activations by $^tBu_2PCH_2CH_2P^tBu_2$ and $^tBu_2PCH_2P^tBu_2$ Di(phosphine) Complexes of Rhodium and Iridium, *Organometallics* **2013**, *32*, 1016-1028.

44. Zuzek, A. A.; Parkin, G. Si–H and Si–C Bond Cleavage Reactions of Silane and Phenylsilanes with $Mo(PMe_3)_6$: Silyl, Hypervalent Silyl, Silane, and Disilane Complexes, *J. Am. Chem. Soc.* **2014**, *136*, 8177-8180.

45. Liu, H.-J.; Landis, C.; Raynaud, C.; Eisenstein, O.; Tilley, T. D. Donor-Promoted 1,2-Hydrogen Migration from Silicon to a Saturated Ruthenium Center and Access to Silaoxiranyl and Silaiminyl Complexes, *J. Am. Chem. Soc.* **2015**, *137*, 9186-9194.

46. Price, J. S.; Emslie, D. J. H.; Britten, J. F. Manganese Silylene Hydride Complexes: Synthesis and Reactivity with Ethylene to Afford Silene Hydride Complexes, *Angew. Chem., Int. Ed.* **2017**, *56*, 6223-6227.

47. Price, J. S.; Emslie, D. J. H.; Vargas-Baca, I.; Britten, J. F. $[(dmpe)_2MnH(C_2H_4)]$ as a Source of a Low-Coordinate Ethyl Manganese(I) Species: Reactions with Primary Silanes, H_2, and Isonitriles, *Organometallics* **2018**, *37*, 3010-3023.

48. Many ^{13}C NMR signals and all ^{29}Si NMR signals were not located due to broadness.

49. These coupling constants are very similar to the $^2J_{H,P}$ coupling of 56.5 Hz in Wilksinon and Girolami's $[(dmpe)_2MnH(C_2H_4)]$, which also contains a hydride ligand apical to a plane formed by two κ_2-dmpe ligands; Girolami, G. S.; Howard, C. G.; Wilkinson, G.; Dawes, H. M.; Thornton-Pett, M.; Motevalli, M.; Hursthouse, M. B. Alkyl, Hydrido, and Tetrahydroaluminato Complexes of Manganese with 1,2-Bis(dimethylphosphino)ethane (dmpe). X-Ray Crystal Structures of $Mn_2(\mu\text{-}C_6H_{11})_2(C_6H_{11})_2(\mu\text{-dmpe})$, $(dmpe)_2Mn(\mu\text{-}H)_2AlH(\mu\text{-}H)_2AlH(\mu\text{-}H_2)Mn(dmpe)_2$, and $Li_4\{MnH(C_2H_4)[CH_2(Me)PCH_2CH_2PMe_2]_2\}_2\cdot 2Et_2O$, *J. Chem. Soc., Dalton Trans.* **1985**, 921-929.

50. For selected examples, see refs. 15, 20, 42,43, and 57.

51. Sakaba, H.; Hirata, T.; Kabuto, C.; Kabuto, K. Synthesis, Structure, and Dynamic Behavior of Tungsten Dihydride Silyl Complexes $Cp^*(CO)_2W(H)_2(SiHPhR)$ (R = Ph, H, Cl), *Organometallics* **2006**, *25*, 5145-5150.

52. Selective deuteration of the metal hydride environment in **3a** was not carried out because the starting complex, **1a**, could not be purified.

53. These hydrosilane exchange reactions also lend some insight into the relative stabilities of the four silyl dihydride complexes; reactions of **3a** with similar excesses of $^nBuSiH_3$ and H_2SiEt_2 yielded $[(dmpe)_2MnH_2(SiH_2{}^nBu)]$ (**4b**) and $[(dmpe)_2MnH_2(SiHEt_2)]$ (**3b**) respectively, but these reactions only proceeded to 90% and 10% conversion respectively. From the reverse perspective, reaction of **3b** with an excess of Ph_2SiH_2 yielded nearly 100% conversion to **3a** overnight at 60 °C. Together, this suggests that the aromatic analogues are thermodynamically favoured over aliphatic analogues.

54. Discussed values are those from the dominant disordered conformer.

55. Murphy, L. J.; Ferguson, M. J.; McDonald, R.; Lumsden, M. D.; Turculet, L. Synthesis of Bis(phosphino)silyl Pincer-Supported Iron Hydrides for the Catalytic Hydrogenation of Alkenes, *Organometallics* **2018**, *37*, 4814-4826.

56. Zuzek, A. A.; Neary, M. C.; Parkin, G. *σ*-Silane, Disilanyl, and [W(μ-H)Si(μ-H)W] Bridging Silylene Complexes *via* the Reactions of $W(PMe_3)_4(\eta^2\text{-}CH_2PMe_2)H$ with Phenylsilanes, *J. Am. Chem. Soc.* **2014**, *136*, 17934-17937.

57. Delpech, F.; Sabo-Etienne, S.; Daran, J.-C.; Chaudret, B.; Hussein, K.; Marsden, C. J.; Barthelat, J.-C. Ruthenium Complexes Containing Two Ru–(η^2-Si–H) Bonds: Synthesis, Spectroscopic Properties, Structural Data, Theoretical Calculations, and Reactivity Studies, *J. Am. Chem. Soc.* **1999**, *121*, 6668-6682.

58. (a) Delpech, F.; Sabo-Etienne, S.; Chaudret, B.; Daran, J.-C. Synthesis and Characterization of Chelating Bis(silane) Complexes $[RuH_2\{(\eta^2\text{-}HSiMe_2)_2X\}(PCy_3)_2]$ (X = C_6H_4, O) Containing Two Ru–(η^2-Si–H) Bonds, *J. Am. Chem. Soc.* **1997**, *119*, 3167-3168. (b) Ayed, T.; Barthelat, J.-C.; Tangour, B.; Pradère, C.; Donnadieu, B.; Grellier, M.; Sabo-Etienne, S. Structure and Bonding in a Disilazane Ruthenium Complex. Catalytic Selective Deuteration of Disilazane, *Organometallics* **2005**, *24*, 3824-3826.

59. The calculated $Si–H_{MnSi}$ distances are different from one another by 0.03-0.05 Å, consistent with a limited degree of second order Jahn-Teller distortion, as described in ref. 7.

60. See refs. 9, 21, 37, and (a) Ng, S. M.; Lau, C. P.; Fan, M.-F.; Lin, Z. Experimental and Theoretical Studies of Highly Fluxional $TpRu(PPh_3)"H_2SiR_3"$ Complexes (Tp = Hydridotris(pyrazolyl)borate), *Organometallics* **1999**, *18*, 2484-2490. It should be noted that examples of dihydrogen silyl complexes have been observed, and some comuptational results have suggested that these complexes should have similar energies to hydrosilane hydride complexes; see ref. 16, (b) Esteruelas, M. A.; Oro, L. A.; Valero, C. Hydrosilylation of Phenylacetylene via an $Os(SiEt_3)(\eta^2\text{-}H_2)$ Intermediate Catalyzed by $OsHCl(CO)(P^iPr_3)_2$, *Organometallics* **1991**, *10*, 462-466., and (c) Lachaize, S.; Caballero, A.; Vendier, L.; Sabo-Etienne, S. Activation of Chlorosilanes at Ruthenium: A Route to Silyl *σ*-Dihydrogen Complexes, *Organometallics* **2007**, *26*, 3713-3721.

61. Luo, Y.-R., Bond Dissociation Energies. In *CRC Handbook of Chemistry and Physics*, 90 ed.; Lide, D., Ed. CRC Press 2010.

62. The experimentally and computationally unobserved *lateralHSi* isomer of dmpe-coordinated **3a-b**, **4a-b**, (or **4b***) would require H_{Mn1}–Mn–Si–X dihedral angles of approximately 60° (×2) and 180° (×1), where X represents any one of the 3 substitutents on silicon, bringing the hydrocarbyl substituent(s) on silicon into closer proximety to the dmpe ligands than in a *lateralH_2* isomer.

63. Keeler, J., *Understanding NMR Spectroscopy*. John Wiley & Sons: New York, 2010, pp 334-335.

64. For examples of these experiments used to determine $J_{Si,H}$, see refs. 20 and 57.

65. For an example of such an experiment used to measure $J_{Si,H}$ in a nonclassical hydrosilane complex, see ref. 22.

66. We were previously unable to determine the sign or magnitude of $J_{Si,H}$ from standard 2D dqf $^1H–^1H$ NMR spectroscopy. Therefore, in our initial report we provded only the experimentally determined magnitude of $J_{Si,H}$ for **2a**; 36Hz determined using 2D $^{29}Si–^1H$ HMBC NMR spectroscopy, and using this method, we were unable to determine the magnitude of $J_{Si,H}$ for **2b**. See reference 47.

67. B. J. Burger, J. E. B., Vacuum Line Techniques for Handling Air-Sensitive Organometallic Compounds. In *Experimental Organometallic Chemistry - A Practicum in Synthesis and Characterization*, American Chemical Society: Washington, D.C., 1987; Vol. 357, pp 79-98.

68. (a) ADF2010, SCM, Theoretical Chemistry, Vrije Universiteit, Amsterdam, The Netherlands, http://www.scm.com; Guerra, C. F.; Snijders, J. G.; te Velde, G.; Baerends, E. J. Towards an order-*N* DFT method, *Theor. Chem. Acc.* **1998**, *99*, 391-403. (b) te Velde, G.; Bickelhaupt, F. M.; Baerends, E. J.; Fonseca Guerra, C.; Van

Gisbergen, S. J. A.; Snijders, J. G.; Ziegler, T. Chemistry with ADF, *J. Comput. Chem.* **2001**, *22*, 931-967.

69. Perdew, J. P.; Burke, K.; Ernzerhof, M. Generalized Gradient Approximation Made Simple, *Phys. Rev. Lett.* **1996**, *77*, 3865-3868.

70. (a) van Lenthe, E.; Baerends, E. J.; Snijders, J. G. Relativistic regular two-component Hamiltonians, *J. Chem. Phys.* **1993**, *99*, 4597-4610. (b) van Lenthe, E.; Baerends, E. J.; Snijders, J. G. Relativistic total energy using regular approximations, *J. Chem. Phys.* **1994**, *101*, 9783-9792. (c) van Lenthe, E.; Snijders, J. G.; Baerends, E. J. The zero-order regular approximation for relativistic effects: The effect of spin-orbit coupling in closed shell molecules, *J. Chem. Phys.* **1996**, *105*, 6505-6516. (d) van Lenthe, E.; van Leeuwen, R.; Baerends, E. J.; Snijders, J. G. Relativistic Regular Two-Component Hamiltonians, *Int. J. Quantum Chem.* **1996**, *57*, 281-293. (e) van Lenthe, E.; Ehlers, A.; Baerends, E. J. Geometry optimizations in the zero order regular approximation for relativistic effects, *J. Chem. Phys.* **1999**, *110*, 8943-8953.

71. (a) Grimme, S.; Antony, J.; Ehrlich, S.; Krieg, H. A consistent and accurate ab initio parametrization of density functional dispersion correction (DFT-D) for the 94 elements H-Pu, *J. Chem. Phys.* **2010**, *132*, 154104. (b) Grimme, S.; Ehrlich, S.; Goerigk, L. Effect of the Damping Function in Dispersion Corrected Density Functional Theory, *J. Comput. Chem.* **2011**, *32*, 1456-1465.

72. (a) Becke, A. D. A multicenter numerical integration scheme for polyatomic molecules, *J. Chem. Phys.* **1988**, *88*, 2547-2553. (b) Franchini, M.; Philipsen, P. H. T.; Visscher, L. The Becke Fuzzy Cells Integration Scheme in the Amsterdam Density Functional Program Suite, *J. Comput. Chem.* **2013**, *34*, 1819-1827.

73. (a) Mayer, I. Charge, Bond Order and Valence in the Ab Initio SCF Theory, *Chem. Phys. Lett.* **1983**, *97*, 270-274. (b) Mayer, I. Charge, Bond Order and Valence in the Ab Initio SCF Theory (Addendum), *Chem. Phys. Lett.* **1985**, *117*, 396. (c) Mayer, I. On Bond Orders and Valences in the *Ab Initio* Quantum Chemical Theory, *Int. J. Quantum Chem.* **1986**, *29*, 73-84. (d) Sannigrahi, A. B.; Kar, T. Three-center bond index, *Chem. Phys. Lett.* **1990**, *173*, 569-572. (e) Bridgeman, A. J.; Cavigliasso, G.; Ireland, L. R.; Rothery, J. The Mayer bond order as a tool in inorganic chemistry, *J. Chem. Soc., Dalton Trans.* **2001**, 2095-2108.

74. (a) Bérces, A.; Dickson, R. M.; Fan, L.; Jacobsen, H.; Swerhone, D.; Ziegler, T. An implementation of the coupled perturbed Kohn-Sham equations: perturbation due to nuclear displacements, *Comput. Phys. Commun.* **1997**, *100*, 247-262. (b) Jacobsen, H.; Bérces, A.; Swerhone, D. P.; Ziegler, T. Analytic second derivatives of molecular energies: a density functional implementation, *Comput. Phys. Commun.* **1997**, *100*, 263-276. (c) Wolff, S. K. Analytical Second Derivatives in the Amsterdam Density Functional Package, *Int. J. Quantum Chem.* **2005**, *104*, 645-659.

75. The SCANFREQ command rescans a specific range of frequencies along a normal mode numerically as described in the ADF manual: https://www.scm.com/doc/ADF/Input/Frequencies.html#scanning-a-range-of-frequencies. Reference for numeric frequency calculations is Fan, L.; Ziegler, T. Application of density-functional theory to infrared absorption intensity calculations on main group molecules, *J. Chem. Phys.* **1992**, *96*, 9005-9012.

76. (a) Autschbach, J.; Ziegler, T. Nuclear spin-spin coupling constants from regular approximate relativistic density functional calculations. I. Formalism and scalar relativistic results for heavy metal compounds, *J. Chem. Phys.* **2000**, *113*, 936-947. (b) Autschbach, J.; Ziegler, T. Nuclear spin-spin coupling constants from regular approximate relativistic density functional calculations. II. Spin-orbit coupling effects and anisotropies., *J. Chem. Phys.* **2000**, *113*, 9410-9418.

77. (a) Grimme, S. Accurate Description of van der Waals Complexes by Density Functional Theory Including Empirical Corrections, *J. Comput. Chem.* **2004**, *25*, 1463-1473. (b) Ernzerhof, M.; Scuseria, G. E. Assessment of the Perdew-Burke-Ernzerhof exchange-correlation functional, *J. Chem. Phys.* **1999**, *110*, 5029-5036.

78. Spaltenstein, E.; Palma, P.; Kreutzer, K. A.; Willoughby, C. A.; Davis, W. M.; Buchwald, S. L. Preparation and X-ray Structure of $Cp_2Ti(Ph_2SiH_2)(PMe_3)$, *J. Am. Chem. Soc.* **1994**, *116*, 10308-10309.

79. (a) Note 29 in; Bulo, R.; Ehlers, A.; Grimme, S.; Lammertsma, K. Vinylphospirane-Phospholene Rearrangements: pericyclic [1,3]-Sigmatropic Shifts or Not?, *J. Am. Chem. Soc.* **2002**, *124*, 13903-13910. (b) Pauncz, R., *Spin Eigenfunctions*. Plenum Press: New York, **1979**. (c) Szabo, A.; Ostlund, N., *Modern Quantum Chemistry*. 1st ed. revised ed. ed.; McGraw_Hill: New York, **1989**.

80. Sheldrick, G. M. A short history of SHELX, *Acta Crystallogr., Sect. A: Found. Crystallogr.* **2008**, *64*, 112-122.

81. Sheldrick, G. M. Crystal structure refinement with SHELXL, *Acta Crystallogr., Sect. C: Cryst. Struct. Chem.* **2015**, *71*, 3-8.

82. Dolomanov, O. V.; Bourhis, L. J.; Gildea, R. J.; Howard, J. A. K.; Puschmann, H. OLEX2: a complete structure solution, refinement and analysis program, *J. Appl. Crystallogr.* **2009**, *42*, 339-341.

83. This chemical shift was determined indirectly from 2D NMR spectroscopy.

84. Determined from 1D TOCSY NMR spectroscopy with excitation of the Si*H* signal.